New $V^{IV}O$-complexes for oxidative desulfurization of refractory sulfur compounds in fuel: synthesis, structure, reactivity trend and mechanistic studies

Tendai O. Dembaremba,[a,*] Isabel Correia,[b] Eric C. Hosten,[a] Maxim L. Kuznetsov,[b] Wilhelmus J. Gerber,[c,*] João C. Pessoa[b,*] Adeniyi S. Ogunlaja,[a] and Zenixole R. Tshentu [a,*]

*Corresponding authors

[a] Department of Chemistry, Nelson Mandela University, P.O. Box 77000, Port-Elizabeth 6031, South Africa.

Emails: olsentodds@gmail.com (T.O.D.) and zenixole.tshentu@mandela.ac.za (Z.R.T.)

Tel: +27 415 042 074

[b] Centro de Química Estrutural, Instituto Superior Técnico, Universidade de Lisboa, Av. Rovisco Pais, 1049-001 Lisboa, Portugal.

Email: joao.pessoa@ist.utl.pt

Tel: +351 218 419 268

[c] Department of Chemistry and Polymer Science, Stellenbosch University, Private Bag X1, Stellenbosch 7602, Western Cape, South Africa.

Email: wgerber@sun.ac.za

Tel: +27 218 082 699

Supplementary information

1. Synthesis methods

1.1. Preparation of the ligands

The ligand precursors; HPIMX, X = -H, -Br, -OMe and $-NO_2$, were prepared by modifying a procedure reported in literature by Gerber *et al*.[58] for related substituted imidazoles. 0.02 mol. of starting material [3.7 g salicyaldehyde for 2'-(2-hydroxyphenyl)imidazole (HPIMH), 4.0 g 5-bromosalicyaldehyde for 2'-(2-hydroxy-5-bromophenyl)imidazole (HPIMBr), 3.0 g 2-hydroxy-5-methoxybenzaldehyde for 2'-(2-hydroxy-5-methoxyphenyl)imidazole (HPIMMeO) and 3.3 g 2-hydroxy-5-nitrobenzaldehyde for 2'-(2-hydroxy-5-nitrophenyl)imidazole ($HPIMNO_2$)] in 25 mL ethanol (except in the case of $HPIMNO_2$ where DMSO was used) was mixed with 5.0 mL of a 40 % aqueous glyoxal solution at 0°C. 10.0 mL of an ice-cold 25 % aqueous ammonia solution was added and stirred for 30 minutes at 0 ºC. The yellow-brown mixtures were then stirred overnight at room temperature. For HPIMBr and $HPIMNO_2$ the precipitate formed was filtered off and washed with water. For HPIMH and HPIMMeO, ethanol was removed using a rotary evaporator and the ligands were extracted from the residue several times using 20 mL aliquots of diethyl ether. The diethyl ether was then removed using a rotary evaporator and the oil obtained was recrystallized from ethyl acetate to afford pure crystals of the ligands.

(a) 2'-(2-Hydroxyphenyl)imidazole (HPIMH)

Yield: 72%. FT-IR: 1554 cm^{-1}, ν (C=N) and 1264 cm^{-1}, phenolic ν (C-O). 1H NMR (300 MHz, CDCl3) δ 7.75 (s, 1H), 7.63 (d, 1H), 7.24 (t, 1H), 7.12 (s, 2H), 7.07 (d, 1H), 6.86 (t, 1H), 5.73 (s,

1H). CHNS Analysis, expected (found) for $C_9H_8N_2O$ (%): C, 67.49 (67.43); H, 5.03 (5.07); N, 17.49 (17.51).

(b) 2'-(2-Hydroxy-5-bromophenyl)imidazole (HPIMBr)

Yield: 83%. FT-IR: 1528 cm^{-1}, ν (C=N) and 1248 cm^{-1}, phenolic ν (C-O). 1H NMR (300 MHz, DMSO) δ 12.44 (s, 1H), 8.09 (s, 1H), 7.37 (dd, 1H), 7.28 (s, 2H), 7.07 (s, 1H), 6.91 (d, 1H). CHNS Analysis, expected (found) for $C_9H_7BrN_2O$ (%): C, 45.22 (45.26); H, 2.95 (2.91); N, 11.72 (11.75).

(c) 2'-(2-Hydroxy-5-methoxyphenyl)imidazole (HPIMMeO)

Yield: 63%. FT-IR: 1532 cm^{-1}, ν (C=N) and 1219 cm^{-1}, phenolic ν (C-O). 1H NMR (300 MHz, CDCl3) δ 7.19 (s, 1H), 7.08 (s, 1H), 7.05 (s, 1H), 7.02 (s, 2H), 6.91 (s, 1H), 6.89 (s, 1H), 6.75 (d, 2H), 3.63 (s, 3H). CHNS Analysis, expected (found) for $C_{10}H_{10}N_2O_2$ (%): C, 63.15 (63.19); H, 5.30 (5.33); N, 14.73 (14.78).

(d) 2'-(2-Hydroxy-5-nitrophenyl)imidazole ($HPIMNO_2$)

Yield: 88%. FT-IR: 1560 cm^{-1}, ν (C=N) and 1300 cm^{-1}, phenolic ν (C-O). 1H NMR (300 MHz, DMSO) δ 13.88 (s, 1H), 8.93 (s, 1H), 8.11 (d, 1H), 7.35 (s, 2H), 7.07 (d, 1H). CHNS Analysis, expected (found) for $C_9H_7N_3O_3$ (%): C, 52.69 (52.72); H, 3.44 (3.43); N, 20.48 (20.46).

1.2. Preparation of complexes

Complexes were prepared from their ligand precursors adapting literature techniques used for similar *bis*-coordinated complexes.[59] To a solution of each ligand precursor in methanol (except in the case of $HPIMNO_2$ where DMSO was used) a solution of two-fold molar quantity of

$V^{IV}OSO_4$ in water was added. Precipitates were formed immediately. These were filtered off and washed with a methanolic solution and allowed to dry to yield their respective complexes.

(a) Oxidovanadium(IV)-2'-(2-hydroxyphenyl)imidazole [$V^{IV}O(PIMH)_2$]

Yield: 62%. FT- IR (ν, cm^{-1}): 1563, ν(C=N); 1148, ν(C-O); 964, ν(V=O); 446, ν(V-N) and 409, ν(V-O). CHNS Analysis, expected (found) for $C_{18}H_{14}N_4O_3V$ (%): C, 56.26 (56.21); H, 3.41 (3.45); N, 14.58 (14.52).

(b) Oxidovanadium(IV)-2'-(2-hydroxyphenyl)imidazole [$V^{IV}O(PIMMeO)_2$]

Yield: 56%. FT- IR (ν, cm^{-1}): 1570, ν(C=N); 1099, ν(C-O); 944, ν(V=O); 466, ν(V-N) and 430, ν(V-O). CHNS Analysis, expected (found) for $C_{20}H_{18}N_4O_5V$ (%): C, 54.06 (53.98); H, 3.86 (3.87); N, 12.61 (12.58).

(c) Oxidovanadium(IV)-2'-(2-hydroxyphenyl)imidazole [$V^{IV}O(PIMBr)_2$]

Yield: 69%. FT- IR (ν, cm^{-1}): 1563, ν(C=N); 1107, ν(C-O); 973, ν(V=O); 464, ν(V-N) and 421, ν(V-O). CHNS Analysis, expected (found) for $C_{18}H_{12}Br_2N_4O_3V$ (%): C, 39.88 (39.84); H, 2.05 (2.07); N, 10.34 (10.32).

(d) Oxidovanadium(IV)-2'-(2-hydroxyphenyl)imidazole [$V^{IV}O(PIMNO_2)_2$]

Yield: 76%. FT- IR (ν, cm^{-1}): 1560, ν(C=N); 1148, ν(C-O); 992, ν(V=O); 482, ν(V-N) and 421, ν(V-O). CHNS Analysis, expected (found) for $C_{18}H_{12}N_6O_7V$ (%): C, 45.59 (45.59); H, 2.34 (2.40); N, 17.72 (17.68).

2. Computational details

The entropic term in solution (S_s) was calculated according to the procedure described by Wertz[67] and Cooper and Ziegler[68] using **Equations 1** to **6**:

$$\Delta S_1 = R \ln V^s{}_{m,liq} \big/ V_{m,gas} \tag{1}$$

$$\Delta S_2 = R \ln V^\circ{}_m \big/ V^s{}_{m,liq} \tag{2}$$

$$\alpha = \frac{S^{\circ s}{}_{liq} - (S^{\circ s}{}_{gas} + R \ln V^s{}_{m,liq} \big/ V_{m,gas})}{(S^{\circ s}{}_{gas} + R \ln V^s{}_{m,liq} \big/ V_{m,gas})} \tag{3}$$

$$S_s = S_g + \otimes S_{sol} = S_g + [\otimes S_1 + \langle (S_g + \otimes S_1) + \otimes S_2] =$$

$$S_g + [(-12.72 \text{ cal/mol·K}) - 0.32(S_g - 12.72 \text{ cal/mol·K}) + 6.37 \text{ cal/mol·K}] \quad (CH_3OH) \tag{4}$$

$$S_g + [(-12.21 \text{ cal/mol·K}) - 0.23(S_g - 12.21 \text{ cal/mol·K}) + 5.87 \text{ cal/mol·K}] \quad (CH_3CN) \tag{5}$$

$$S_g + [(-10.16 \text{ cal/mol·K}) - 0.15(S_g - 10.16 \text{ cal/mol·K}) + 3.81 \text{ cal/mol·K}] \quad (\text{heptane}) \tag{6}$$

where S_g is the gas-phase entropy of the solute, ΔS_{sol} is the solvation entropy, $S^{\circ,s}{}_{liq}$, $S^{\circ,s}{}_{gas}$ and $V^s{}_{m,liq}$ are the standard entropies and molar volumes of the solvent in the liquid or gas phases (127.2/149.6/328.57 and 239.9/245.5/427.98 J/mol•K and 40.46/52.16/146.51 mL/mol, respectively, for methanol/acetonitrile/heptane), $V_{m,gas}$ is the molar volume of the ideal gas at 25 °C (24450 mL/mol), $V^\circ{}_m$ is the molar volume of the solution that correspond to the standard conditions (1000 mL/mol). The enthalpies and Gibbs free energies in solution (H_s and G_s, respectively) were estimated using the **Equations 7** and **8**:

$$H_s = E_s(6\text{-}311{+}G^*) + H_g(6\text{-}31G^*) - E_g(6\text{-}31G^*) \tag{7}$$

$$G_s = H_s - TS_s \tag{8}$$

where E_s and E_g are the total energies in solution and the gas phase and H_g is the gas-phase enthalpy calculated at the corresponding level.

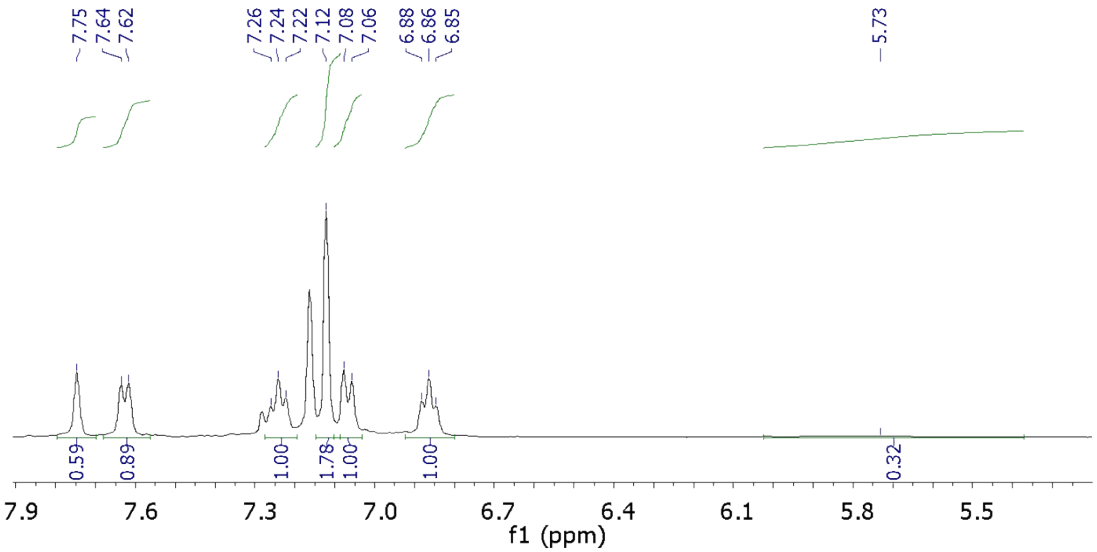

Figure S1. ^{1}H NMR of 2'-(2-hydroxyphenyl)imidazole (HPIMH).

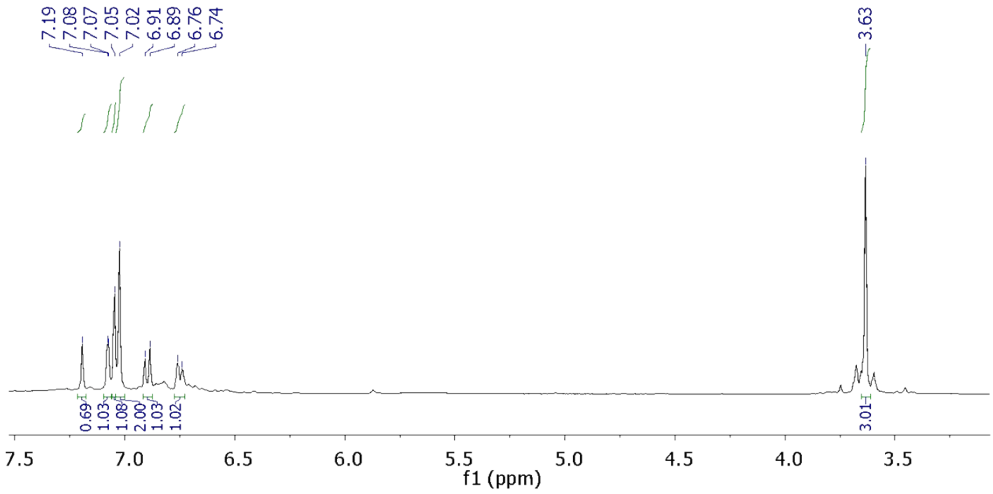

Figure S2. ^{1}H NMR of 2'-(2-hydroxy-5-methoxyphenyl)imidazole (HPIMMeO).

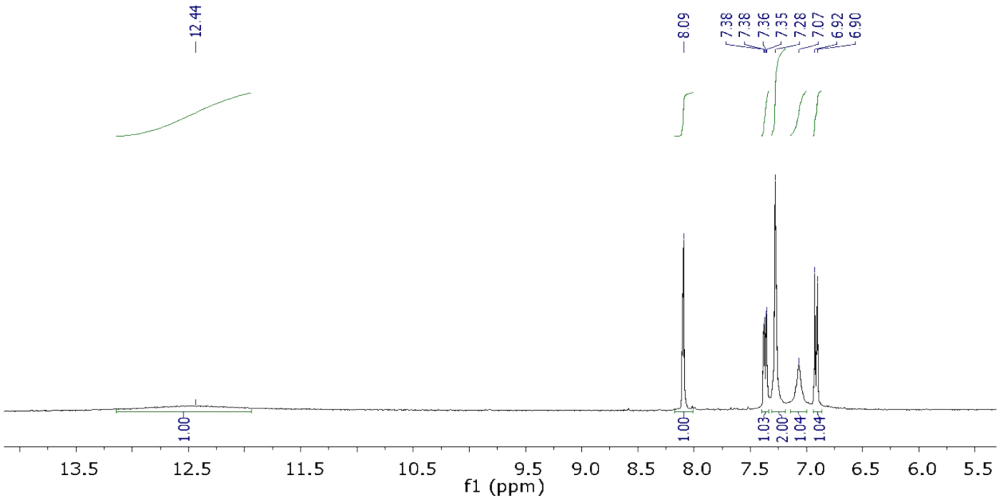

Figure S3. ^{1}H NMR of 2'-(2-hydroxy-5-bromophenyl)imidazole (HPIMBr).

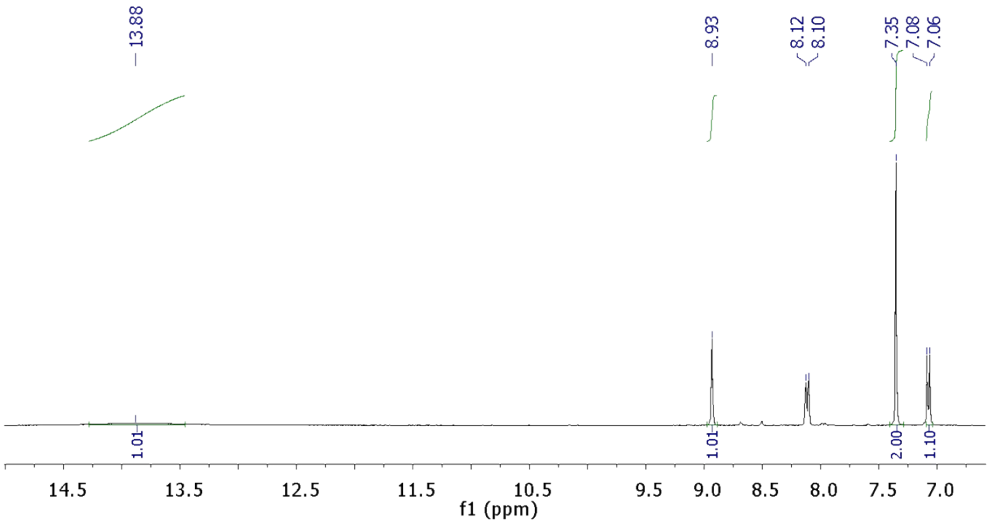

Figure S4. ^{1}H NMR of 2'-(2-hydroxy-5-nitrophenyl)imidazole ($HPIMNO_2$).

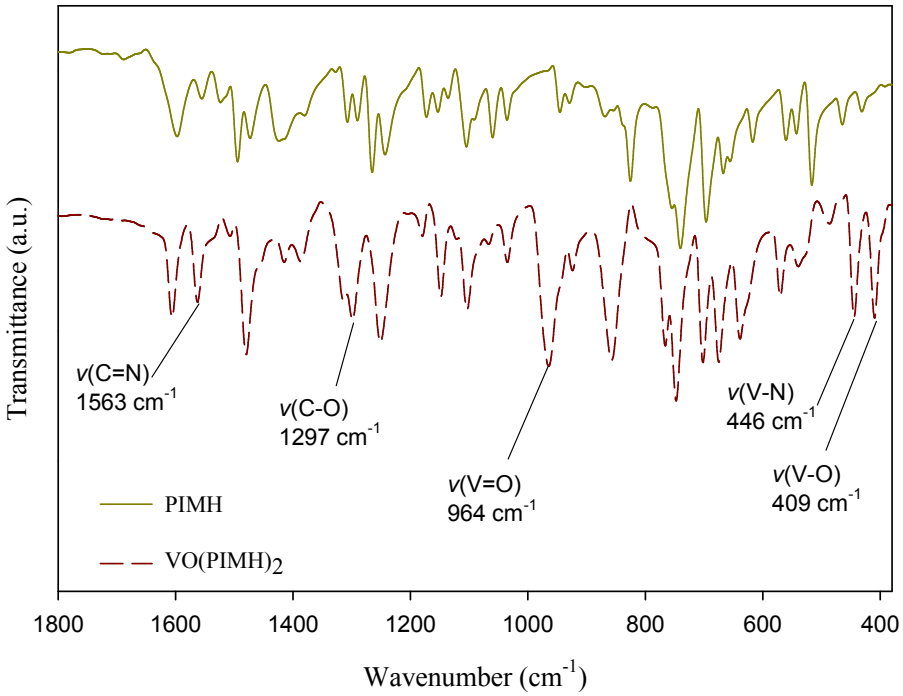

Figure S5. FT-IR spectra of HPIMH and its complex [$V^{IV}O(PIMH)_2$].

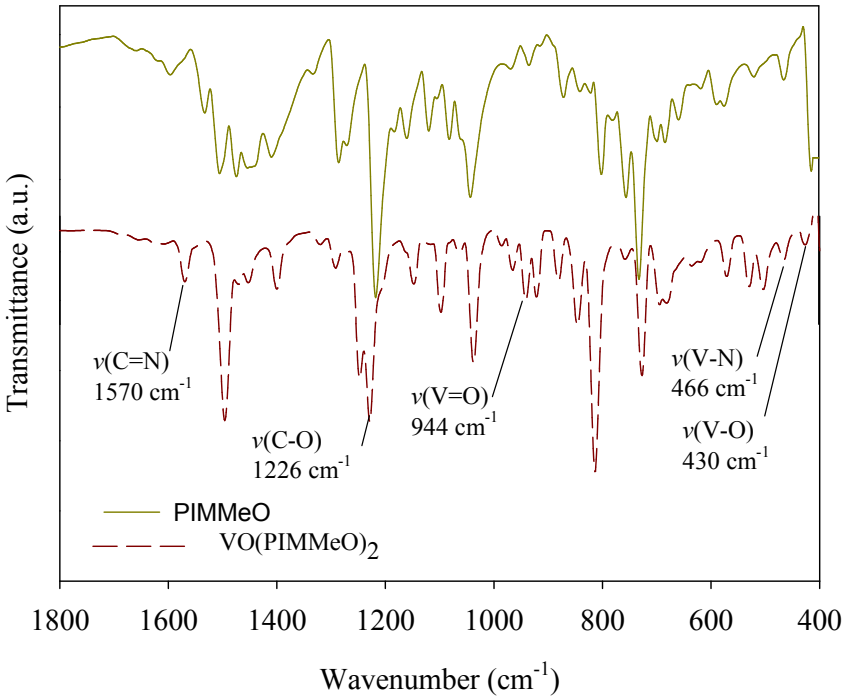

Figure S6. FT-IR spectra of HPIMMeO and its complex [$V^{IV}O(PIMMeO)_2$].

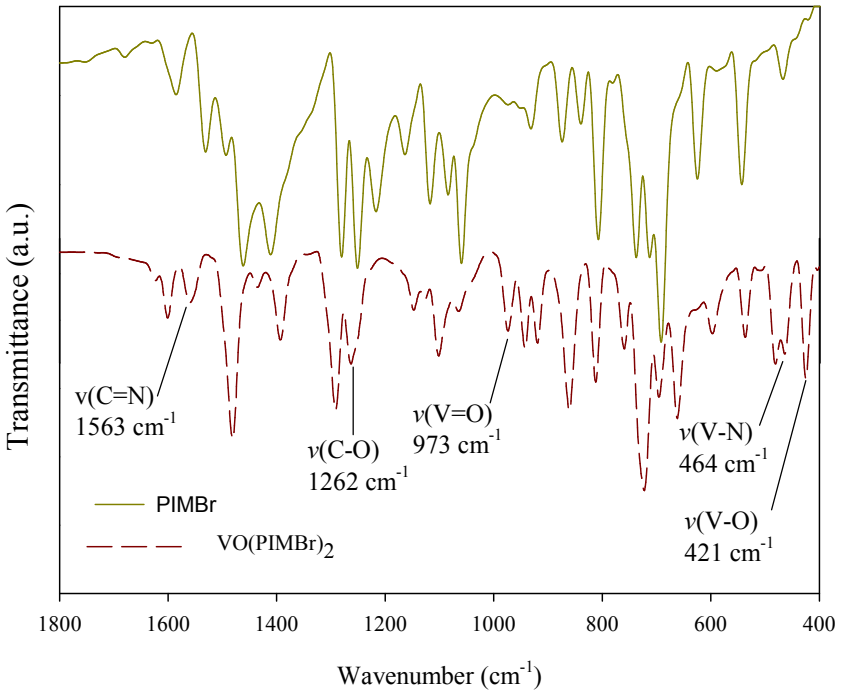

Figure S7. FT-IR spectra of HPIMBr and its complex [$V^{IV}O(PIMBr)_2$].

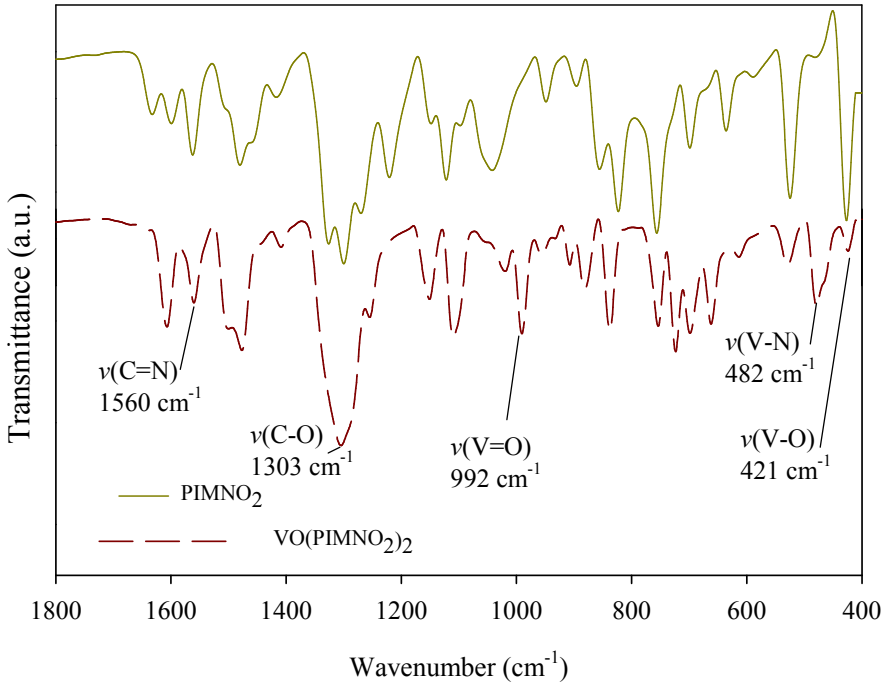

Figure S8. FT-IR spectra of $HPIMNO_2$ and its complex $[V^{IV}O(PIMNO_2)_2]$.

Table S1. FT-IR tentative assignments for important bands in the oxidovanadium(IV) complexes.

Compound	**Wavenumbers (cm^{-1})**				
	ν(C=N)	ν(C-O)	ν(V=O)	ν(V-N)	ν(V-O)
$[V^{IV}O(PIMH)_2]$	1563	1148	964	446	409
$[V^{IV}O(PIMMeO)_2]$	1570	1099	944	466	430
$[V^{IV}O(PIMBr)_2]$	1563	1107	973	464	421
$[V^{IV}O(PIMNO_2)_2]$	1560	1148	992	482	421

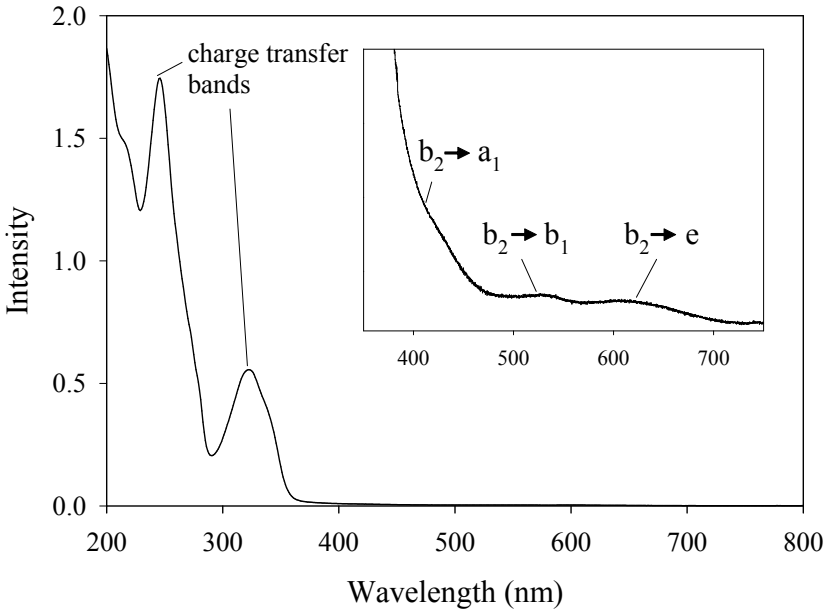

Figure S9. UV-Vis spectrum of [$V^{IV}O(PIMH)_2$]. The insert is an enlargement of the d-d transition region.

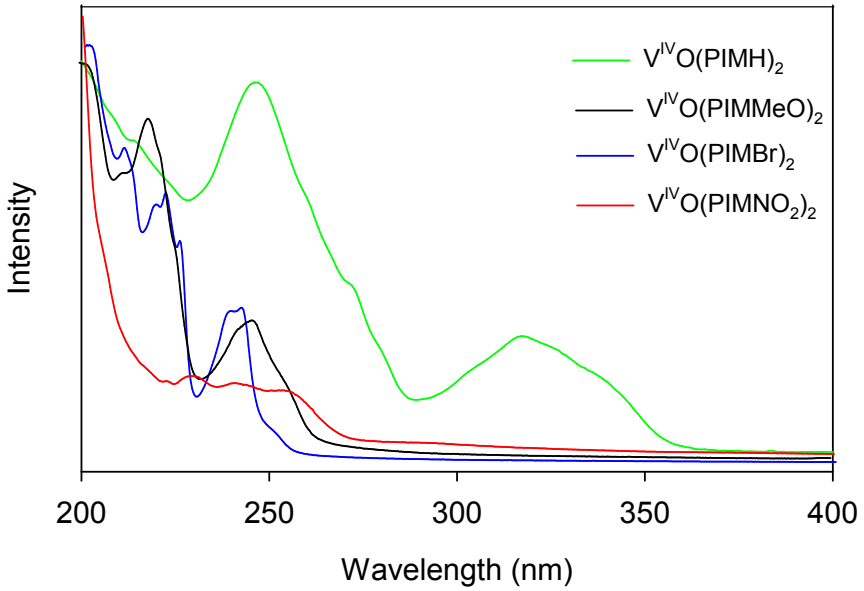

Figure S10. UV-Vis spectra of [$V^{IV}O(PIMH)_2$], [$V^{IV}O(PIMMeO)_2$], [$V^{IV}O(PIMBr)_2$] and [$V^{IV}O(PIMNO_2)_2$] showing the charge transfer bands.

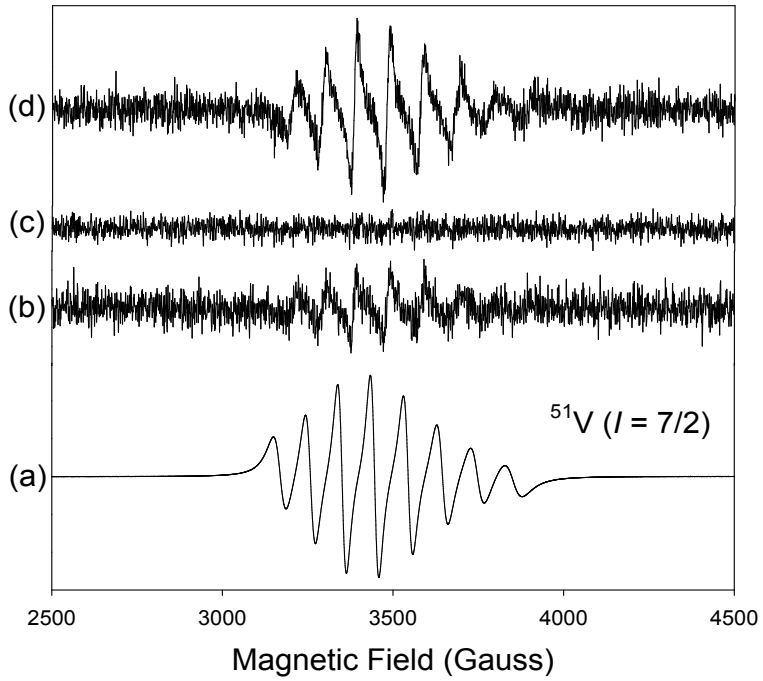

Figure S11. Changes in the EPR spectrum; (a) 0.100 M [$V^{IV}O(PIMH)_2$] in DMF, (b and c) upon addition of 3 times mole eq. 0.526 M *t*-BuOOH and (d) overnight after adding DBT.

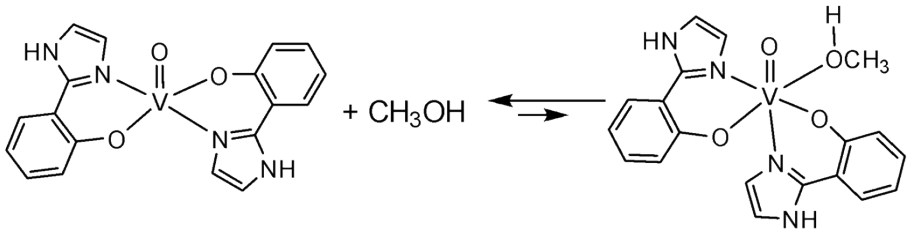

Scheme S1. Two plausible complexes that may form upon dissolving [$V^{IV}O(PIMH)_2$] in MeOH. The one shown on the left, $[V^{IV}O(PIMH)_2]^{EQ}$, is significantly more stable; the DFT calculated ΔG^{o} value for the reaction in MeOH being +11.4 kcal·mol^{-1}.

Table S2. Selected crystal data for $[V^{IV}O(PIMH)_2]$, $[V^{V}O(PIMH)(PIMH_2)]$, $[V^{IV}O(PIMBr)_2]$ and $[V^{IV}O(PIMNO_2)_2]$.

Compound	**$[V^{IV}O(PIMH)_2]$**	**$[V^{V}O(PIMH)(PIMH_2)]$**	**$[V^{IV}O(PIMBr)_2]$**	**$[V^{IV}O(PIMNO_2)_2]$**
Empirical formula	$C_{18}H_{14}N_4O_3V$ $2(C_2H_6OS)$	$C_{18}H_{15}N_4O_4V$	$C_{18}H_{12}Br_2N_4O_3V$ $2(C_2H_6OS)$	$C_{18}H_{12}N_6O_7V$ (C_2H_6OS)
Formula	541.53	402.28	699.33	553.40
Crystal	dark blue-green	yellow	dark blue-green	dark blue-green
Crystal	monoclinic	orthorhombic	orthorhombic	monoclinic
Space group	*P*21/c (No. 14)	*P*212121 (No. 19)	*P*212121 (No. 19)	*P*21/c (No. 14)
Temp. (K)	200	200	200	200
a, b, c (Å)	15.8192(9) 10.5686(6) 14.8615(8)	7.2579(3) 13.8117(5) 16.2980(6)	15.3157(7) 15.8806(8) 22.1939(13)	13.8817(5) 13.0525(5) 13.1235(5)
α, γ, β (^{0})	90, 94.964(2), 90	90, 90, 90	90, 90, 90	90, 108.646(2), 90
V (Å^3)	2475.3(2)	1633.78(11)	5398.1(5)	2253.05(15)
Z	4	4	8	4
ρ_{calc} (g/cm3)	1.453	1.635	1.721	1.632
Radiation	0.71073	0.71073	0.71073	0.71073
Total	43888	15488	56689	26442
Unique reflections	6170	4064	13338	5606
R, wR2, S	0.0369, 0.1025, 1.07	0.0284, 0.0758, 1.06	0.0453, 0.1212, 1.04	0.0447, 0.1286, 1.06
*CCDC	1908640	1908641	1908642	1908643

*CCDC 1908640-1908643 contains the supplementary crystallographic data for this paper. These data can be obtained free of charge from The Cambridge Crystallographic Data Centre via www.ccdc.cam.ac.uk/structures

Table S3. Selected bond lengths (Å) and angles (º) for $[V^{IV}O(PIMH)_2]$, $[V^{V}O_2(PIMH)(PIMH_2)]$,$[V^{IV}O(PIMBr)_2]$ and $[V^{IV}O(PIMNO_2)_2]$.

$[V^{IV}O(PIMH)_2]$		**$[V^{V}O_2(PIMH)(PIMH_2)]$**		**$[V^{IV}O(PIMBr)_2]$**		**$[V^{IV}O(PIMNO_2)_2]$**	
V(1)-O(1)	1.6101(13)	V(1)-O(1)	1.636(2)	V(1)-O(1)	1.594(5)	V(1)-O(3)	1.6143(18)
V(1)-O(2)	1.9141(13)	V(1)-O(2)	1.635(2)	V(1)-O(11)	1.917(4)	V(1)-O(11)	1.908(2)
V(1)-O(3)	1.9023(12)	V(1)-O(11)	1.949(2)	V(1)-O(21)	1.920(3)	V(1)-O(21)	1.9126(18)
V(1)-N(21)	2.0620(15)	V(1)-O(21)	1.9608(17)	V(1)-N(11)	2.075(5)	V(1)-N(11)	2.0586(19)
V(1)-N(31)	2.0617(15)	V(1)-N(22)	2.084(2)	V(1)-N(21)	2.064(5)	V(1)-N(21)	2.0639(19)
O(1)-V(1)-O(2)	109.90(6)	O(1)-V(1)-O(2)	106.71(11)	O(1)-V(1)-O(11)	109.11(19)	O(3)-V(1)-O(11)	108.63(10)
O(1)-V(1)-O(3)	113.16(6)	O(1)-V(1)-O(11)	102.51(9)	O(1)-V(1)-O(21)	112.2(2)	O(3)-V(1)-O(21)	108.95(9)
O(1)-V(1)-N(21)	103.26(6)	O(1)-V(1)-O(21)	111.35(9)	O(1)-V(1)-N(11)	100.5(2)	O(3)-V(1)-N(11)	105.65(8)
O(1)-V(1)-N(31)	104.39(6)	O(1)-V(1)-N(22)	97.91(9)	O(1)-V(1)-N(21)	101.0(2)	O(3)-V(1)-N(21)	103.07(8)
O(2)-V(1)-O(3)	136.92(6)	O(2)-V(1)-O(21)	141.58(10)	O(11)-V(1)-O(21)	138.69(16)	O(11)-V(1)-O(21)	142.41(8)
N(21)-V(1)-N(31)	152.35(6)	O(11)-V(1)-N(22)	155.00(8)	N(11)-V(1)-N(21)	158.46(19)	N(11)-V(1)-N(21)	151.29(8)
Average ligand bite angle	85.22^0	Ligand bite angle	80.86^0	Average ligand bite angle	86.00^0	Average ligand bite angle	85.90^0

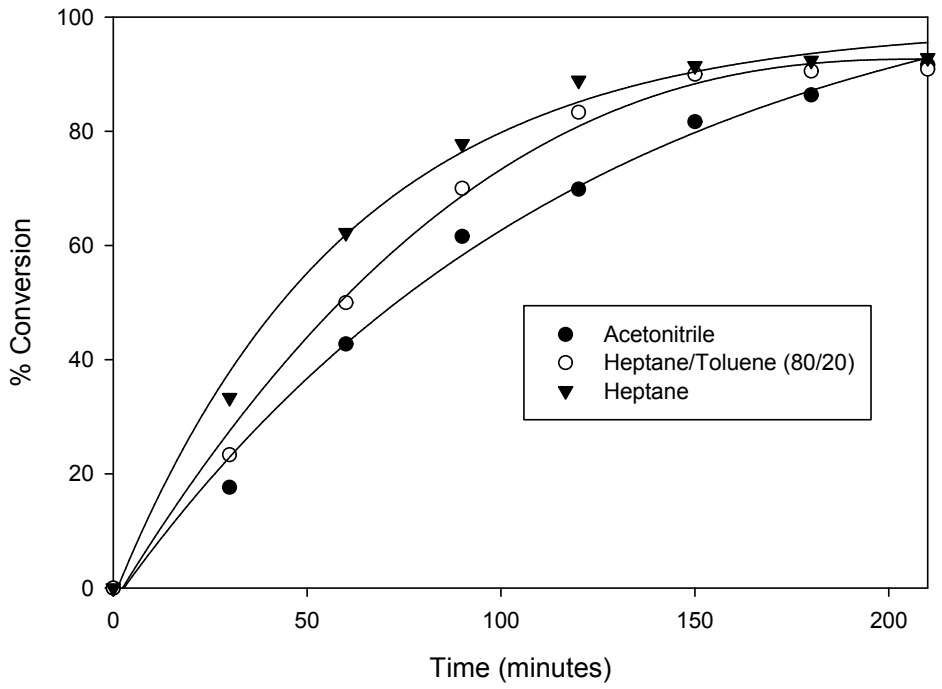

Figure S12. Comparing the activity of PIMH in acetonitrile, heptane and heptane/toluene (80:20). Conditions used 100 mg (0.543 mmol) of DBT, 2.0 mL (10.5 mmol) of t-BuOOH and 6.5 μmol of pre-catalyst in 10 mL of solvent at 60^0C.

Table S4. Vanadium species observed by ESI(+)-MS [a] Compound $[V^{IV}O(PIMH)_2]$ dissolved in methanol except when stated otherwise.

Species proposed	**Predicted masses (m/z)**	**Observed masses (m/z)**	**Comments**
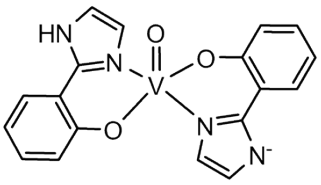	ESI-MS(-): 384.04 385.05 386.05	ESI-MS(-): 384.15 385.2 386.2	**Figure S13A-D** (below). $[V^{IV}O(PIMH)_2]^-$: the initial complex without an H-atom.
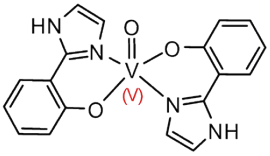	385.05 386.05 387.06	385.13 386.14 387.17	**Figure S14B** (below). $[V^{V}O(PIMH)_2]^+$: the initial complex but with V(V) instead of V(IV).
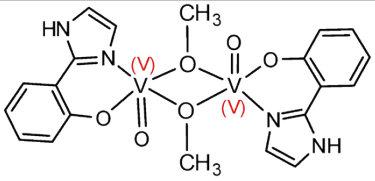	m/z = 514.03 = 257.02	257.04	**Figure S13B** (below). Dimeric complex with two CH_3O^- ligands.
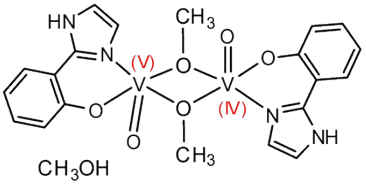	546.05 547.06 548.06	545.52 (Fig. S13F) 545.47; 546.54; 547.5 (Fig. ESI-3B)	One possible assignment of the peaks at m/z = ~545.5 in CH_3CN and also observed in methanol.
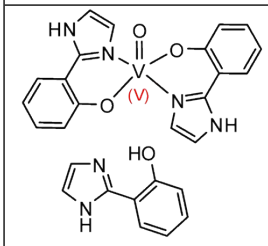	545.11 546.12 547.12	545.47 546.54 547.5 (Fig. ESI-3)	**Figures S13F** and **S14**(below) Another possible assignment of the peaks at m/z = ~545.5 5 in CH_3CN and also observed in methanol.

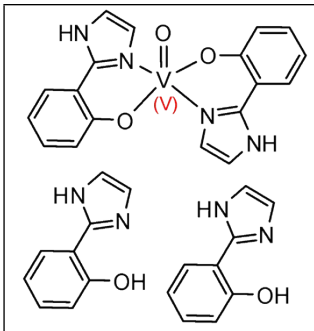	705.18 706.18 707.18	705.79 706.83 707.8	**Figures S14** and **S15A, B** (below) One possible assignment of the peaks at m/z = 705.2
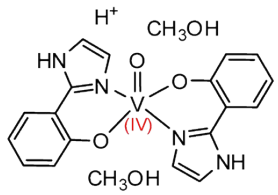	450.11 451.11 452.12	450.11 452.1 453.1	**Figures S14** and **S15A, B** (below). $[V^{IV}O(PIMH)_2]$, with two MeOH and one moiety protonated.
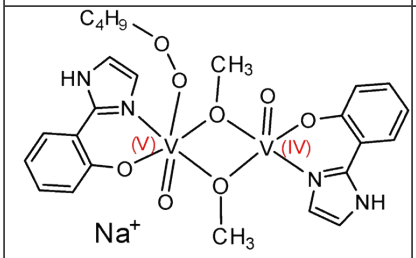	626.08 627.08 629.08	626.49 627.5 628.5	**Figures S14** and **S15A, B** (below). Dinuclear mixed-valence complex with two bridging CH_3O^- and one t-BuOO$^-$ ligands. Very tentative assignment.
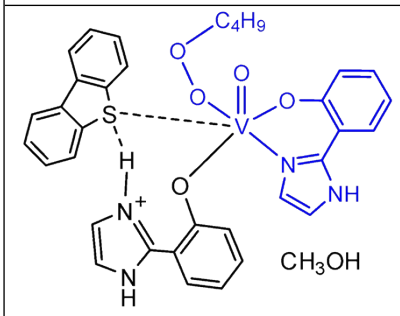 Or, e.g. 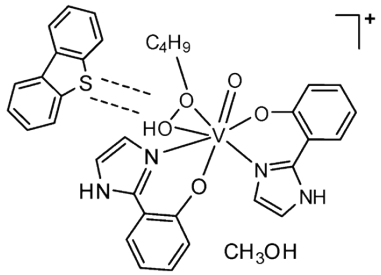	691.18 692.18 693.19	691.43 Very low relative intensity	**Figure S15C** (below). Very tentative assignment of a species including $[V^{IV}O(PIMH)_2(t\text{-}BuOO)]^+$ and a DBT molecule somewhere interacting with it. The MeOH may be coordinated to V(V) or not. Note that the m/z values of radical species corresponding to these structures, such as c-DBT• in Scheme 2, do not differ from the m/z values of these species.

[a] Only the 1st row corresponds to ESI-MS(-).

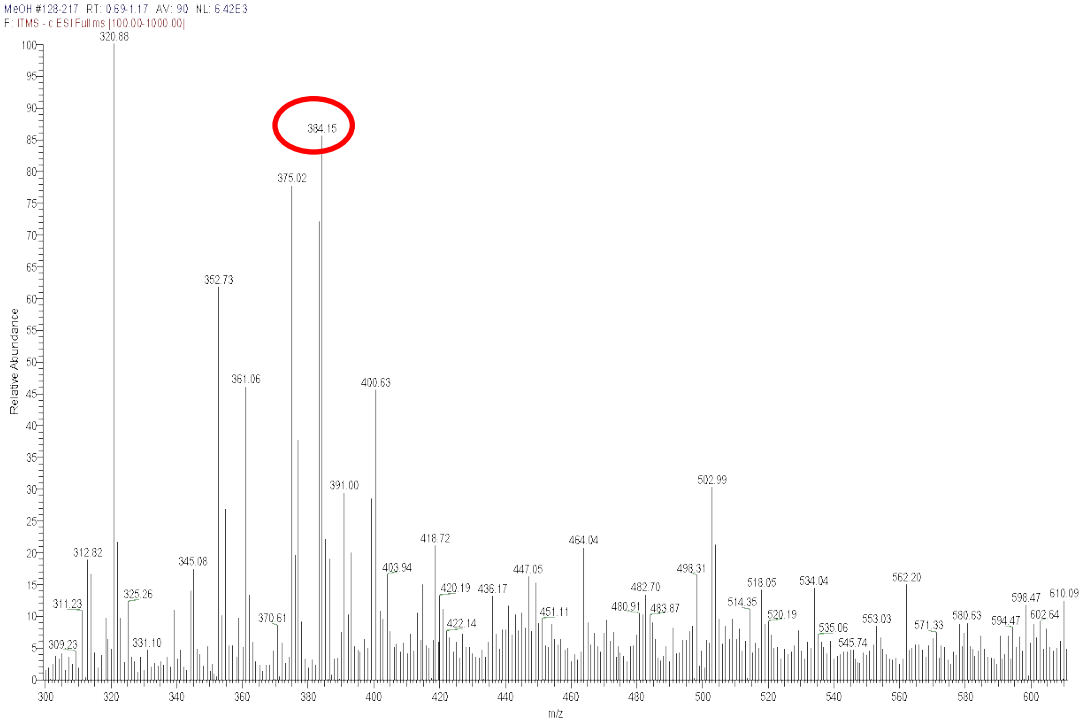

Figure S13A. $[V^{IV}O(PIMH)_2]$ in methanol after 48 h of dissolution.

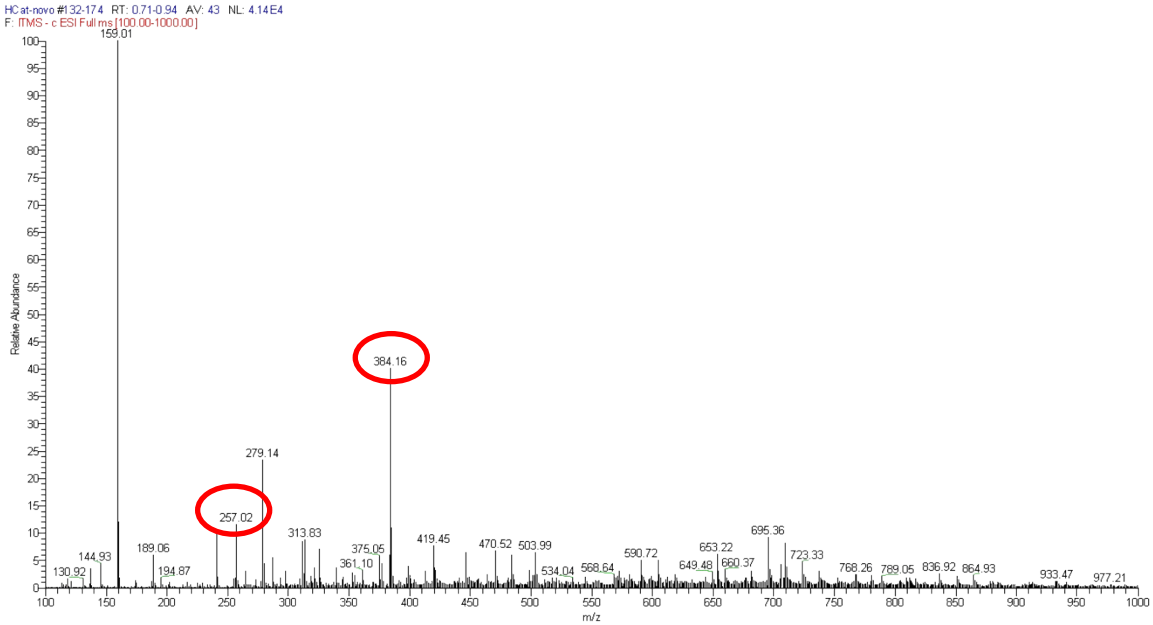

Figure S13B. ESI-MS(-) of $[V^{IV}O(PIMH)_2]$ in methanol a few minutes after dissolution (peak at m/z = 384.16).

Fig. S13C. ESI-MS(+) [$V^{IV}O(PIMH)_2$] in methanol after 48 h dissolution (peak at m/z = 385.13).

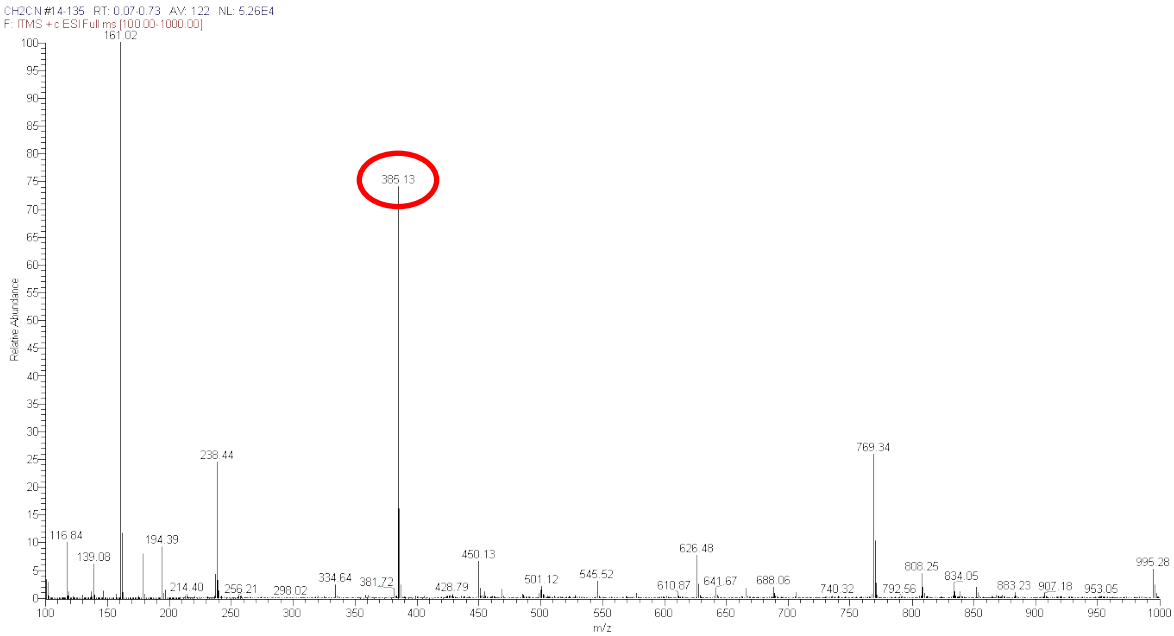

Fig. S13D. ESI-MS(+) of [$V^{IV}O(PIMH)_2$] in methanol after 48 h dissolution (peak at m/z = 385.13).

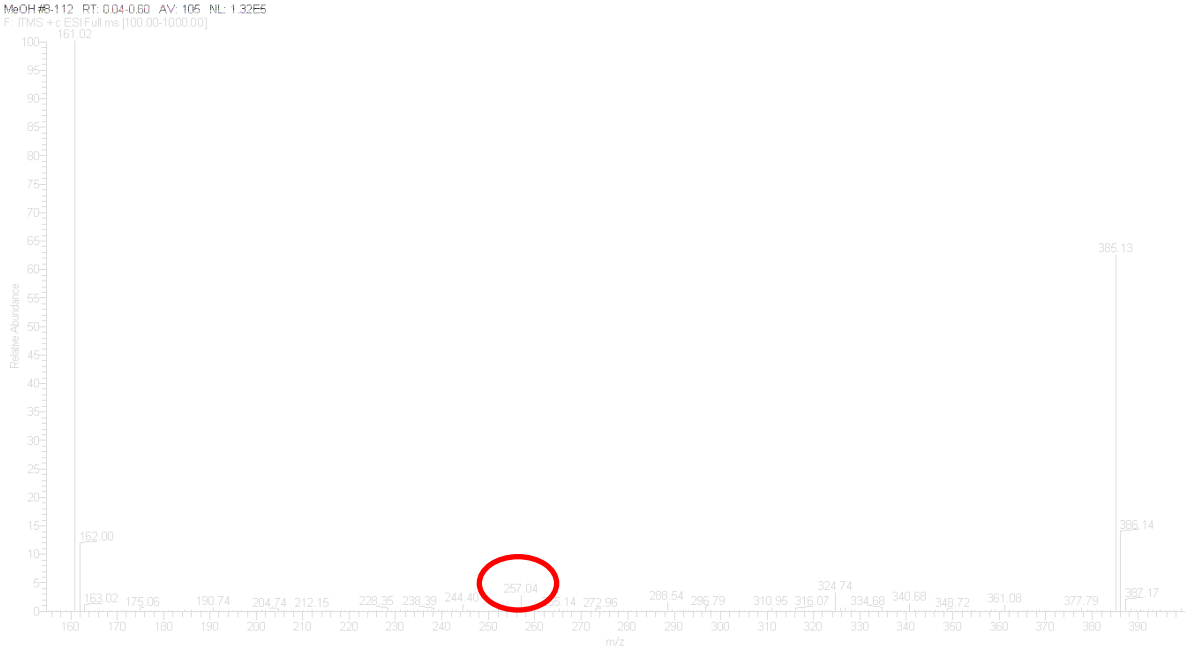

Fig. S13E. ESI-MS(+) of $[V^{IV}O(PIMH)_2]$ in methanol a few minutes after dissolution (peak at m/z = 257.04).

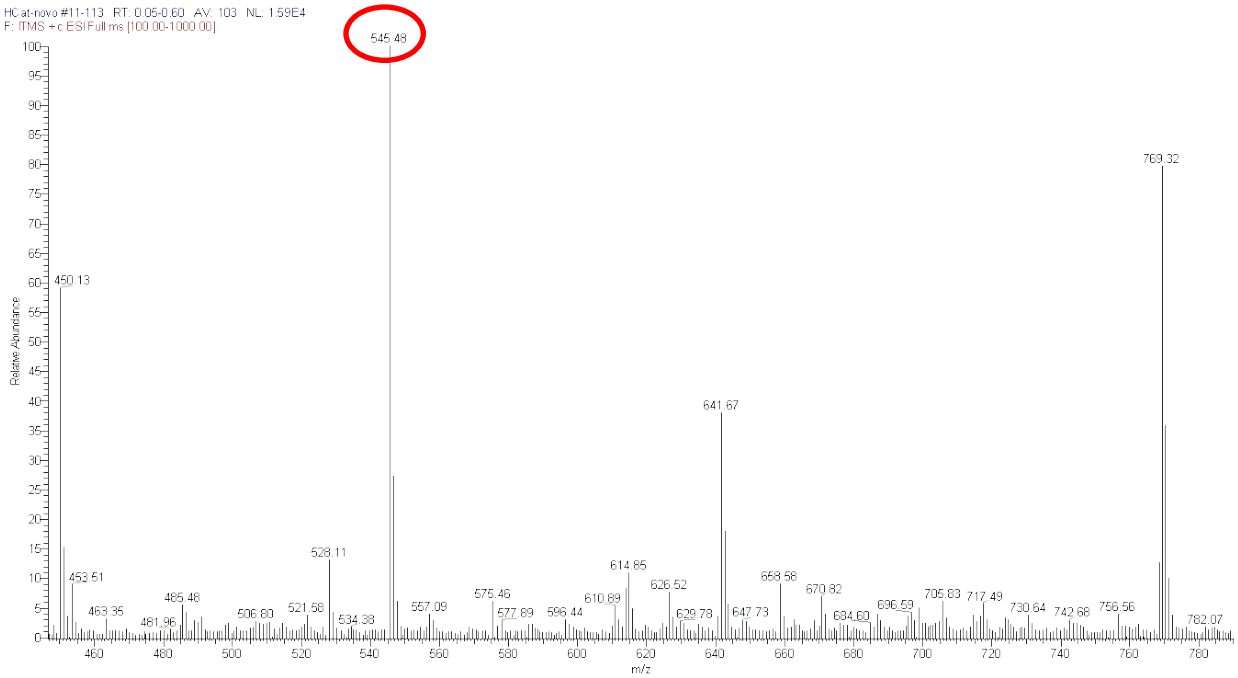

Fig. S13F. ESI-MS(+) of $[V^{IV}O(PIMH)_2]$ in methanol a few minutes after dissolution (peak at m/z = 545.48).

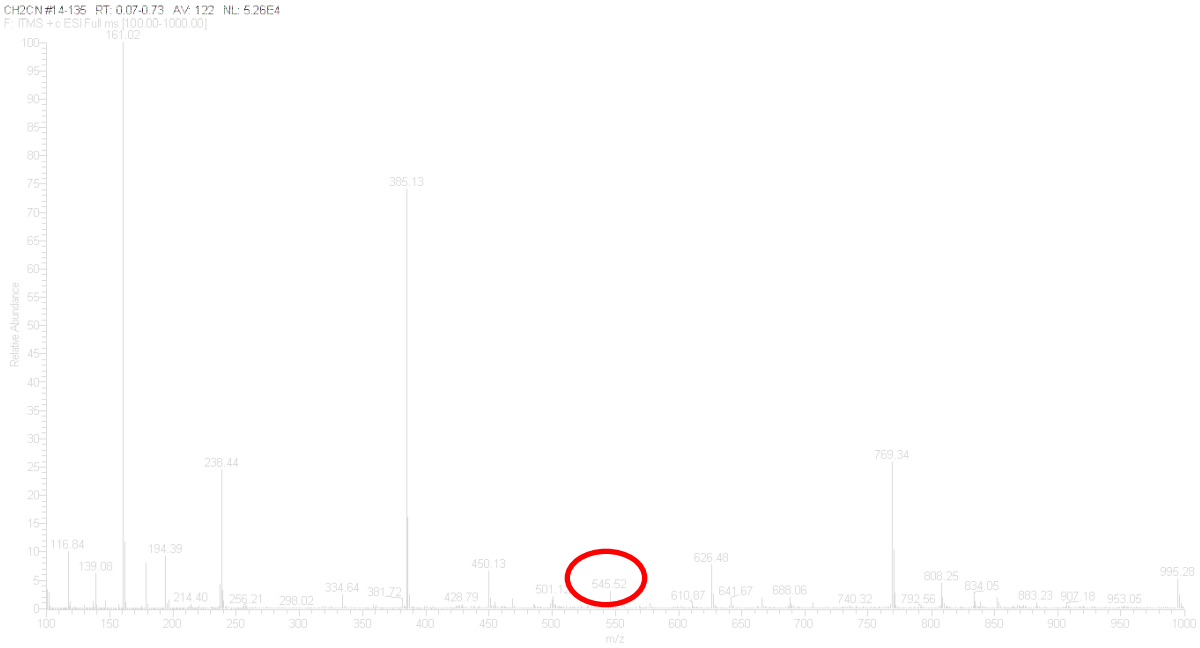

Fig. 14A. ESI-MS(+) of $[V^{IV}O(PIMH)_2]$ in CH_3CN after 48 h dissolution (peak at m/z = 545.52).

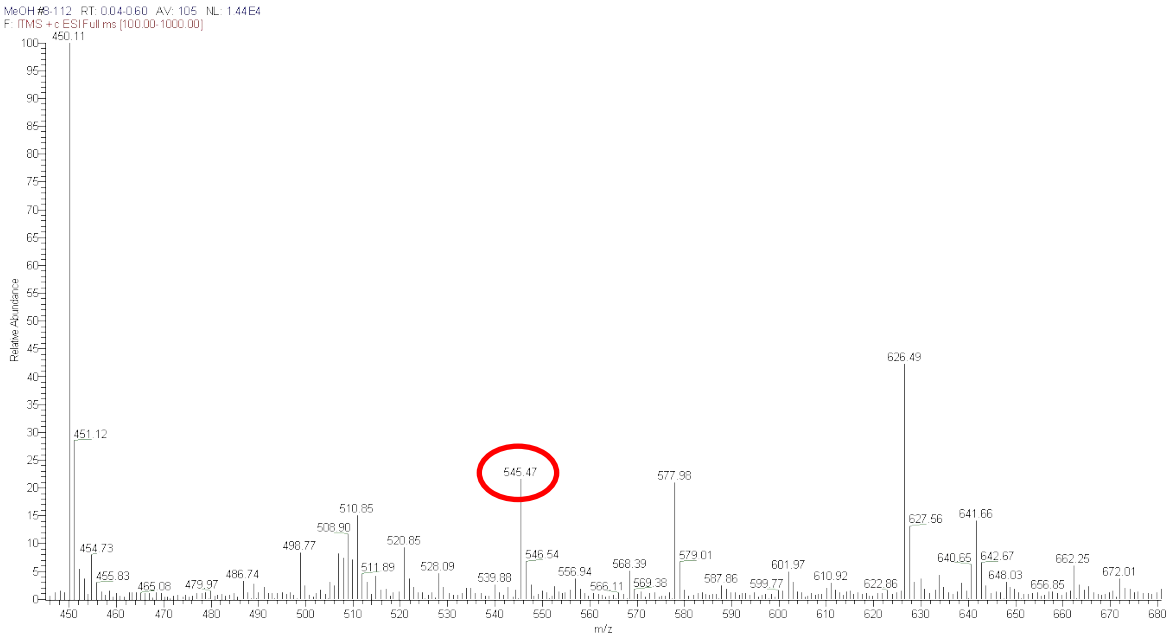

Fig. S14B. ESI-MS(+) of $[V^{IV}O(PIMH)_2]$ in CH_3CN after 48 h dissolution (peak at m/z = 545.47).

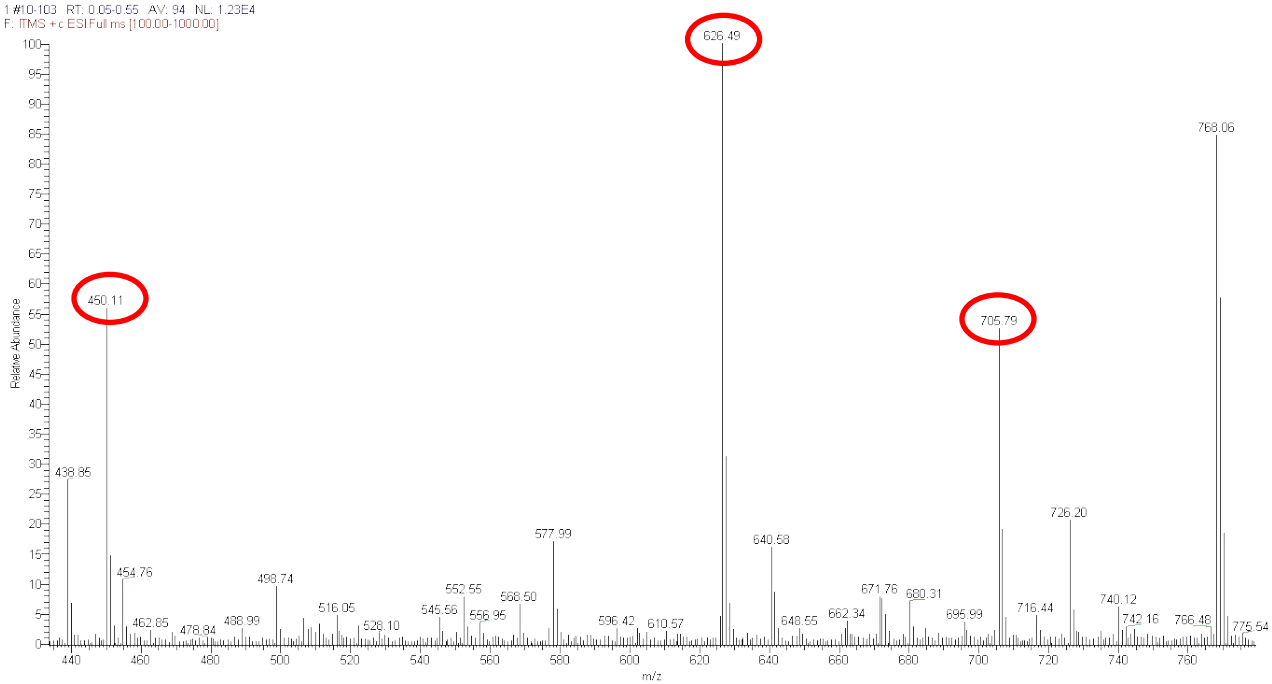

Fig. S15A. ESI-MS(+) of [$V^{IV}O(PIMH)_2$] in methanol after adding 1 equivalent of t-BuOOH (several peaks emphasized).

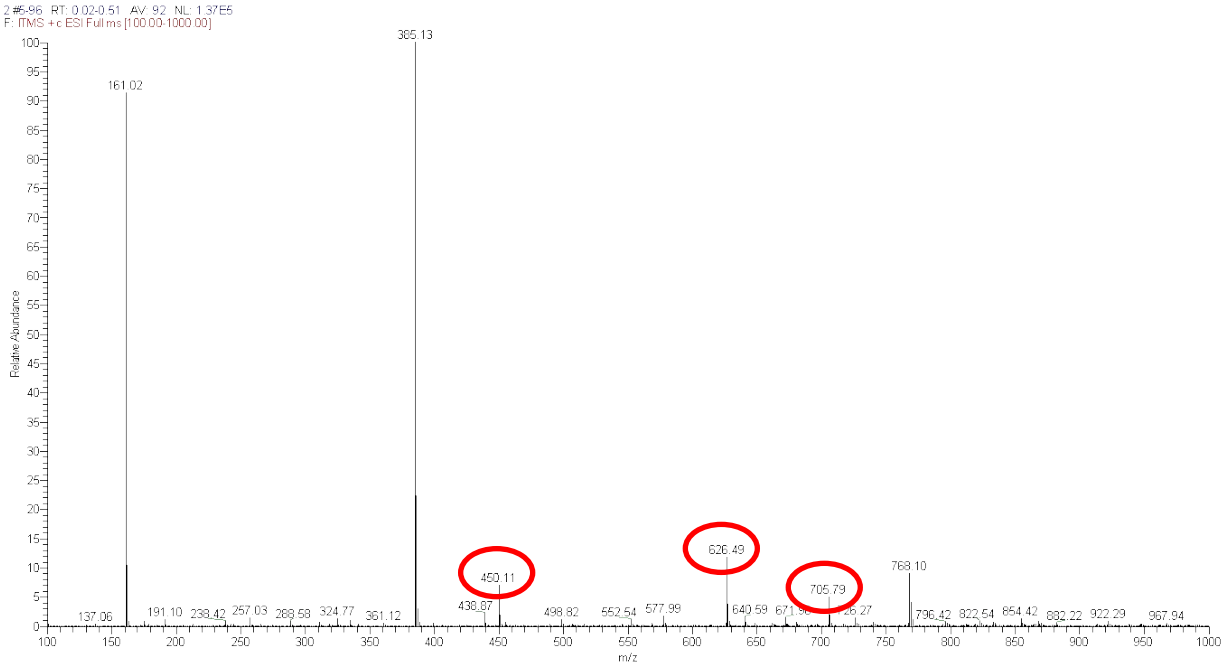

Fig. S15B. ESI-MS(+) of [$V^{IV}O(PIMH)_2$] in methanol after adding 2 equivalents of t-BuOOH (several peaks emphasized).

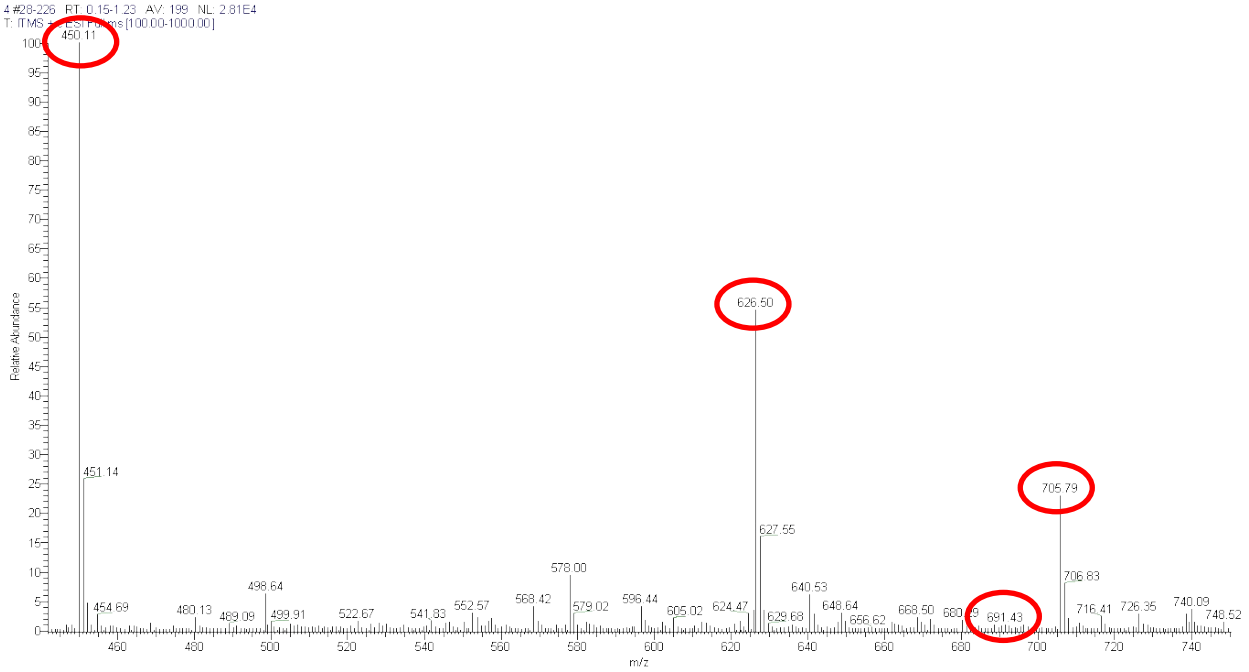

Fig. S15C. ESI-MS(+) of $[V^{IV}O(PIMH)_2]$ in methanol after adding 2 equivalents of t-BuOOH and 2 equivalents of dibenzothiophenes (DBT) (several peaks emphasized, namely the one at m/z = 691.43).

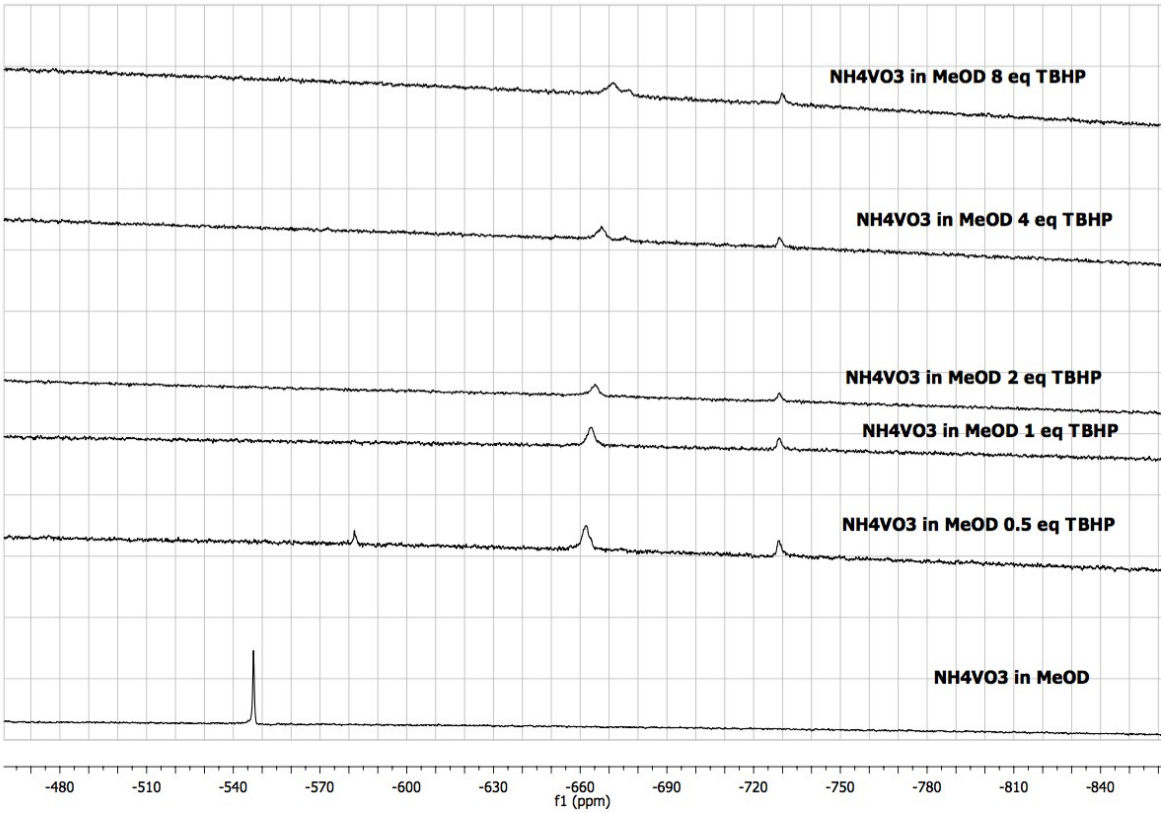

Figure S16. ^{51}V NMR spectra of $NH_4V^VO_3$ in MeOD-d_4 (7.00 mM) after additions of a solution of *t*-BuOOH (0.73M).

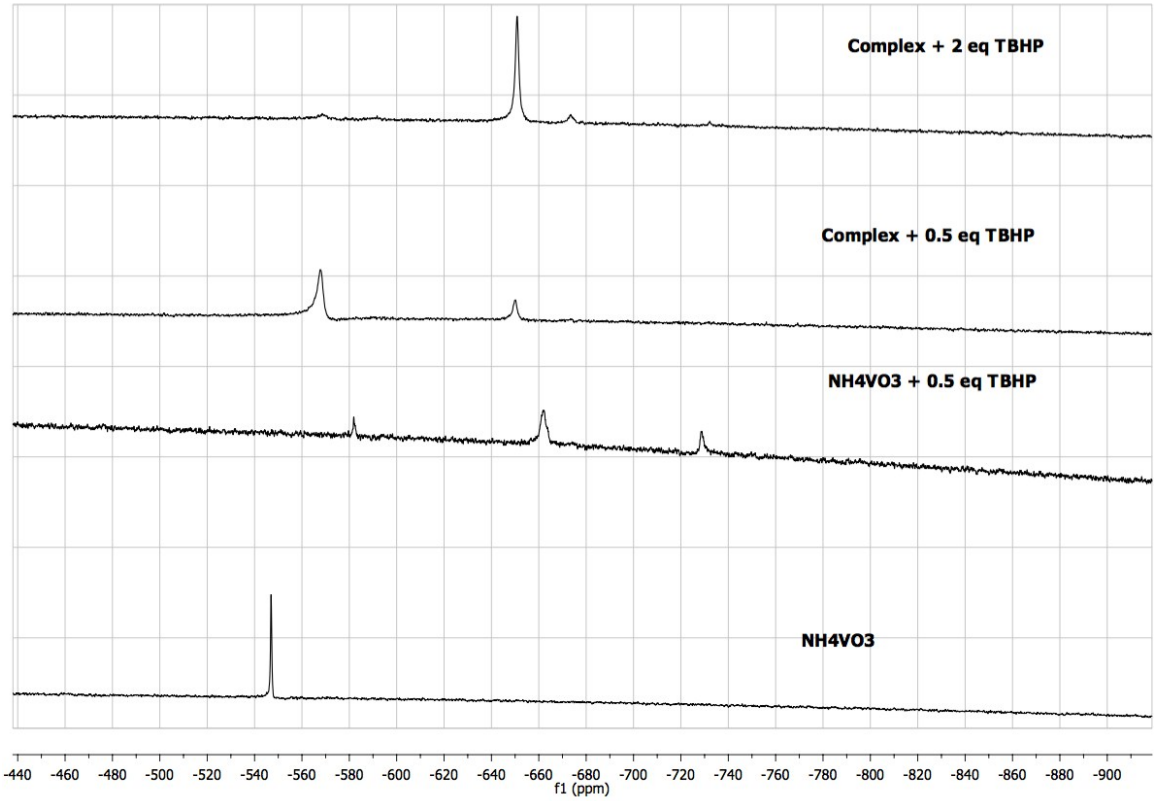

Figure S17. Comparison of the ^{51}V NMR spectra measured for the complex $[V^{IV}O(PIMH)_2]$ (7.00 mM) in MeOH-d_4 and of $NH_4V^VO_3$ after additions of the oxidant. The corresponding δ_V values of oxidoperoxidovanadium(V) clearly differ.

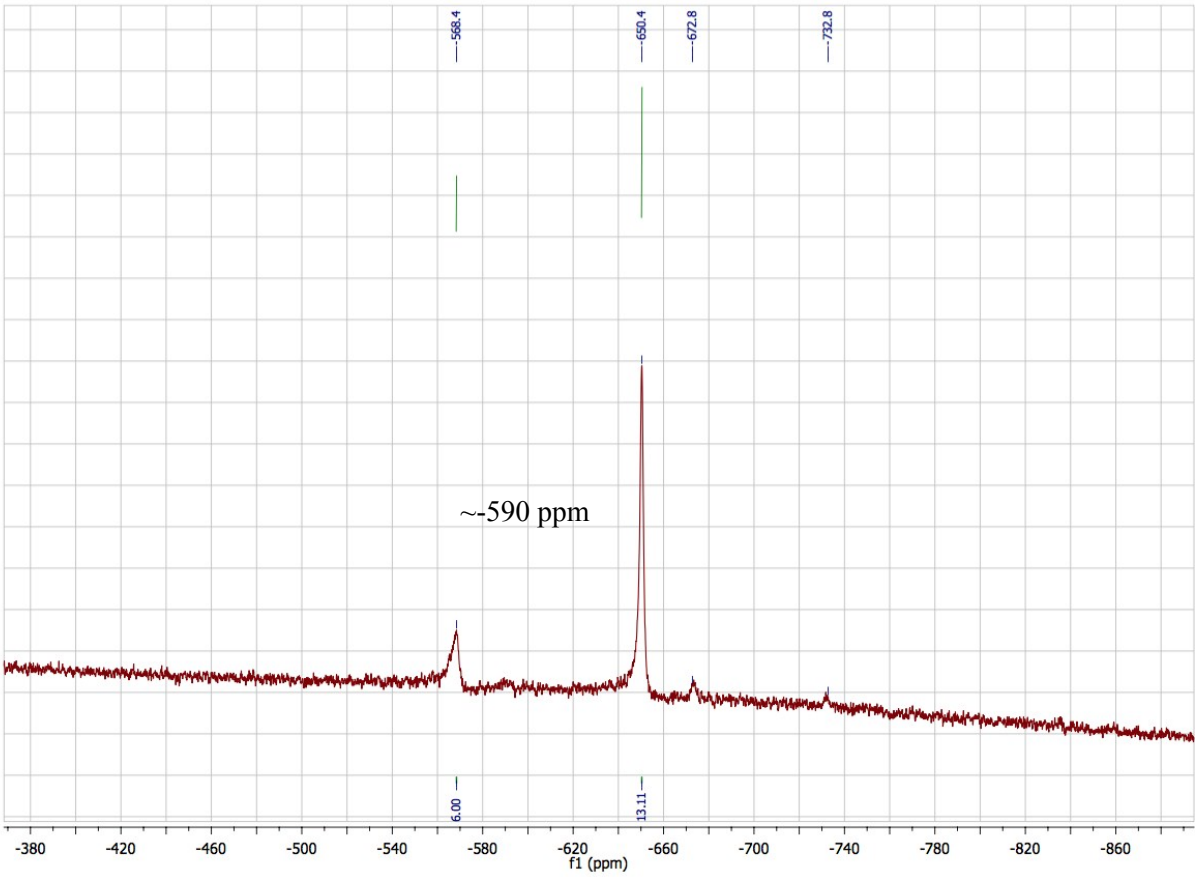

Figure S18. ^{51}V NMR spectrum of the complex [$V^{IV}O(PIMH)_2$] (5 mM) in MeOH-d_4 with 1 eq. *t*-BuOOH. A low intensity resonance is detected at δ_V ca. -590 ppm.

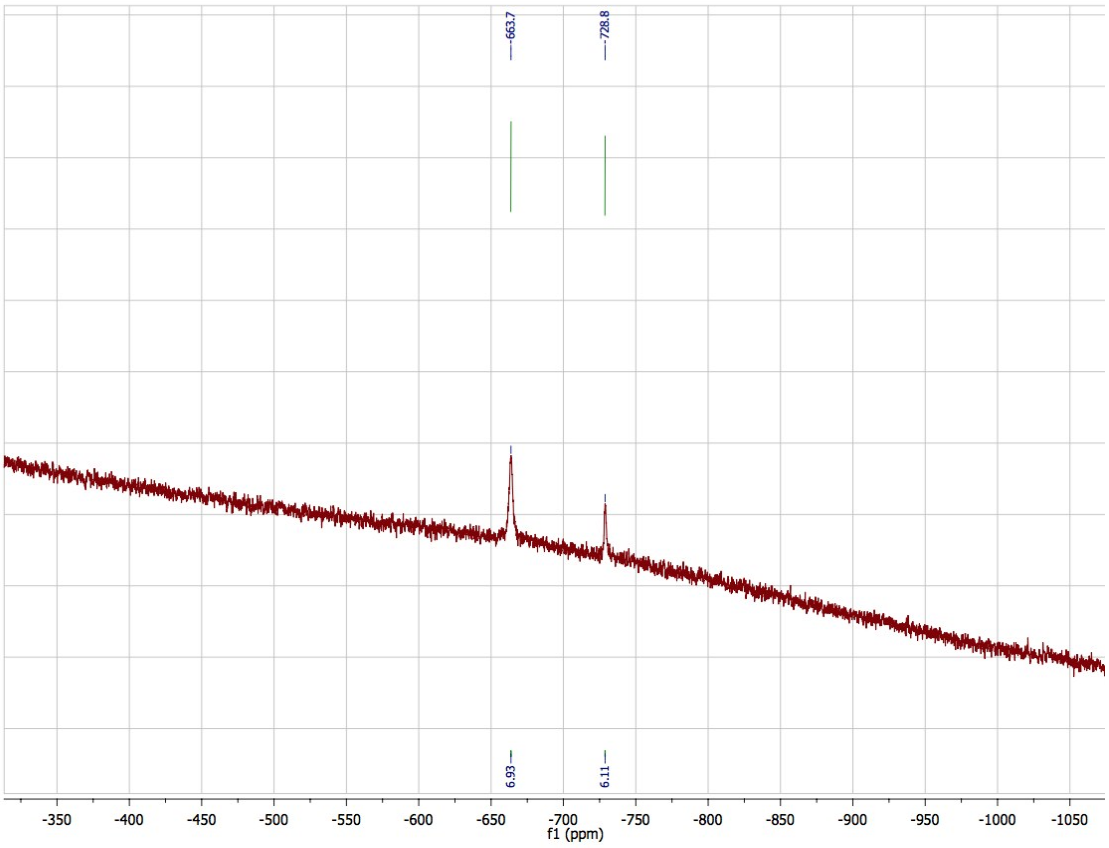

Figure S19. ^{51}V NMR spectrum of $NH_4V^VO_3$ (7 mM) in MeOH-d_4 with 1 eq. *t*-BuOOH.

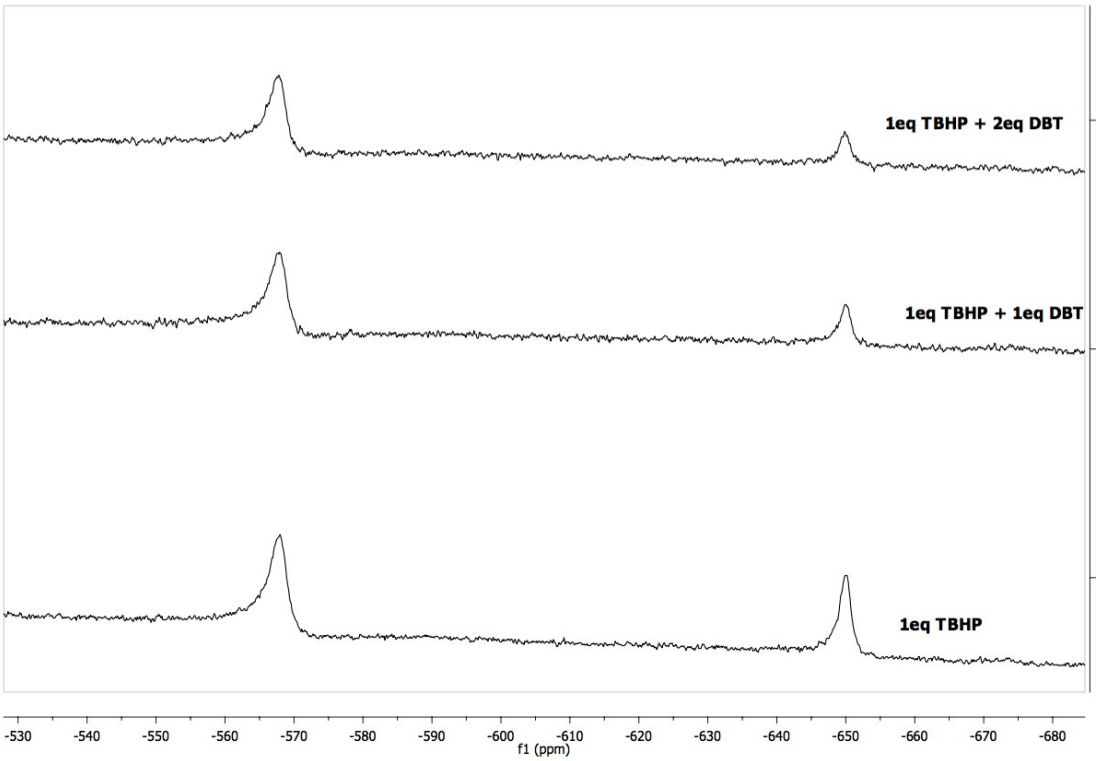

Figure S20. ^{51}V NMR spectra of solutions containing $[V^{IV}O(PIMH)_2]$ (5 mM), 1 eq of *t*-BuOOH) and 0, 1 or 2 eq of DBT (substrate added at room temperature), waiting a few minutes before measuring the spectra. The intensity of all peaks appears to decrease upon additions of DBT.

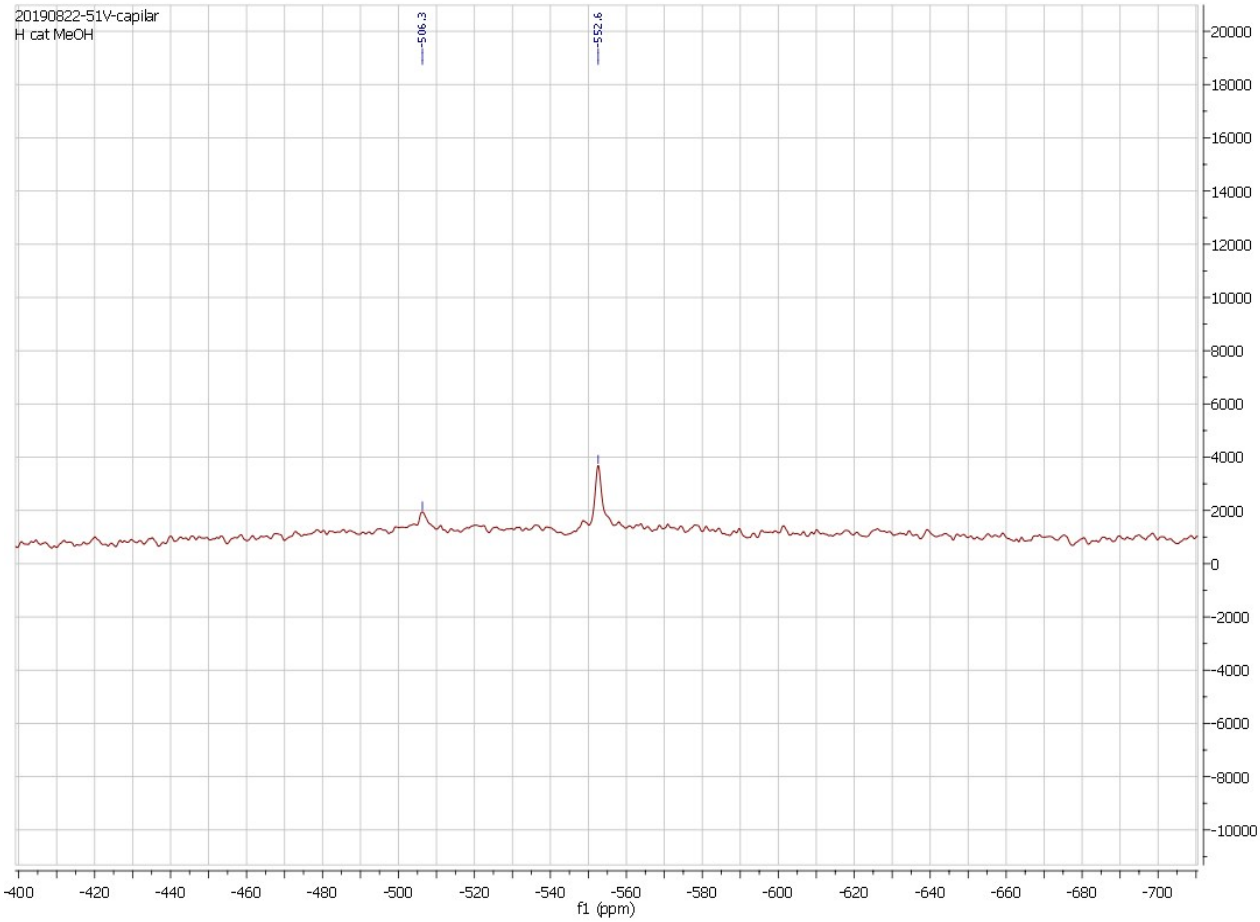

Figure S21. ^{51}V NMR spectra of solutions in MeOH:toluene (90:10) containing $[V^{IV}O(PIMH)_2]$ (concentration < 3 mM) after several hours in contact with air. Peaks are detected at δ_V = -506.3 and -552.6 ppm.

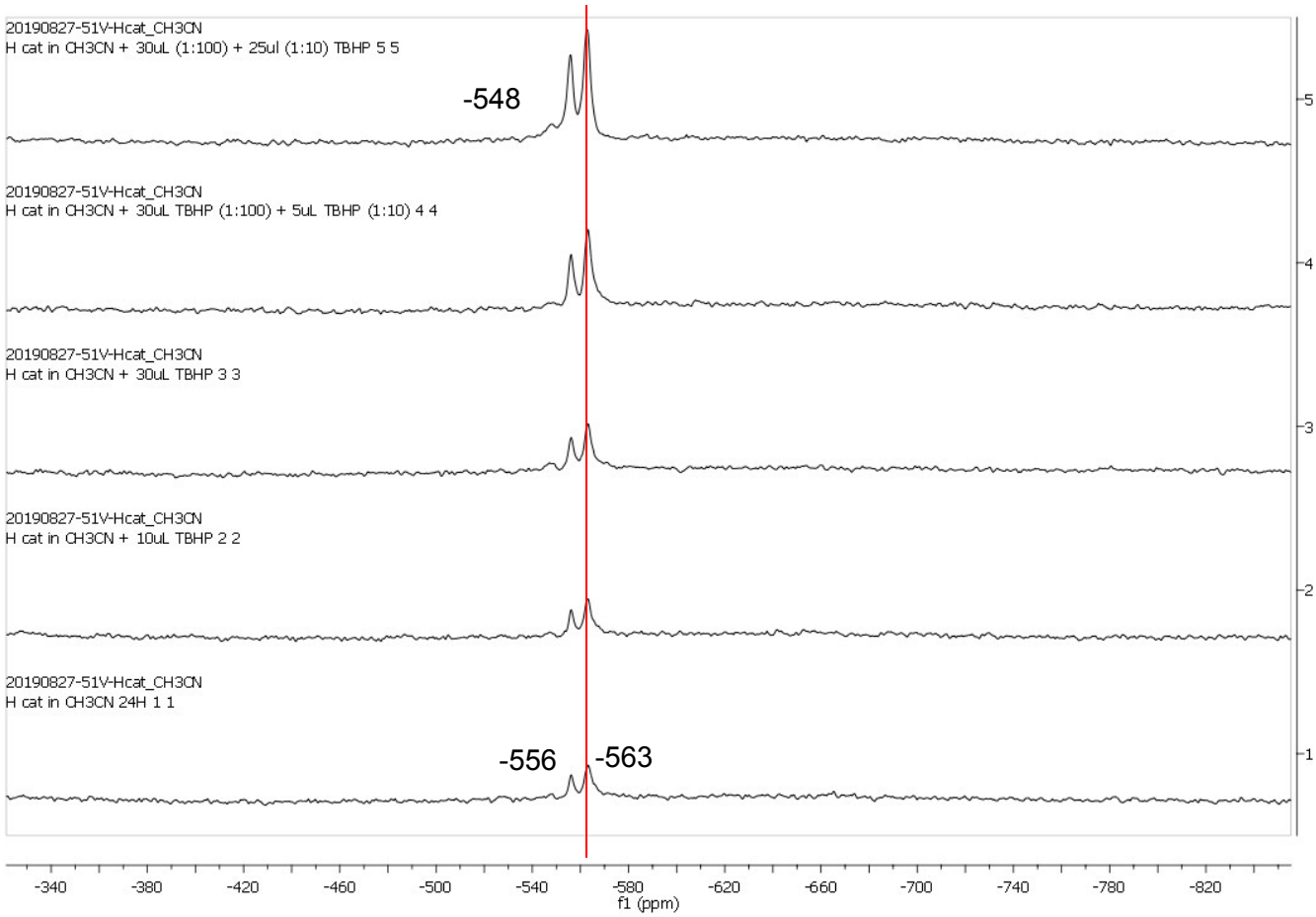

Figure S22. ^{51}V NMR spectra of solutions containing $[V^{IV}O(PIMH)_2]$ (concentration < 3 mM) in CH_3CN:toluene (90:10) after ca. 24 h in air and upon successive additions of *t*-BuOOH. Peaks are detected at δ_V = -556 and -563 ppm, probably two isomers of V(V)-PIMH complexes. After adding high amounts of *t*-BuOOH a small peak is detected at -548, probably due to vanadate(V).

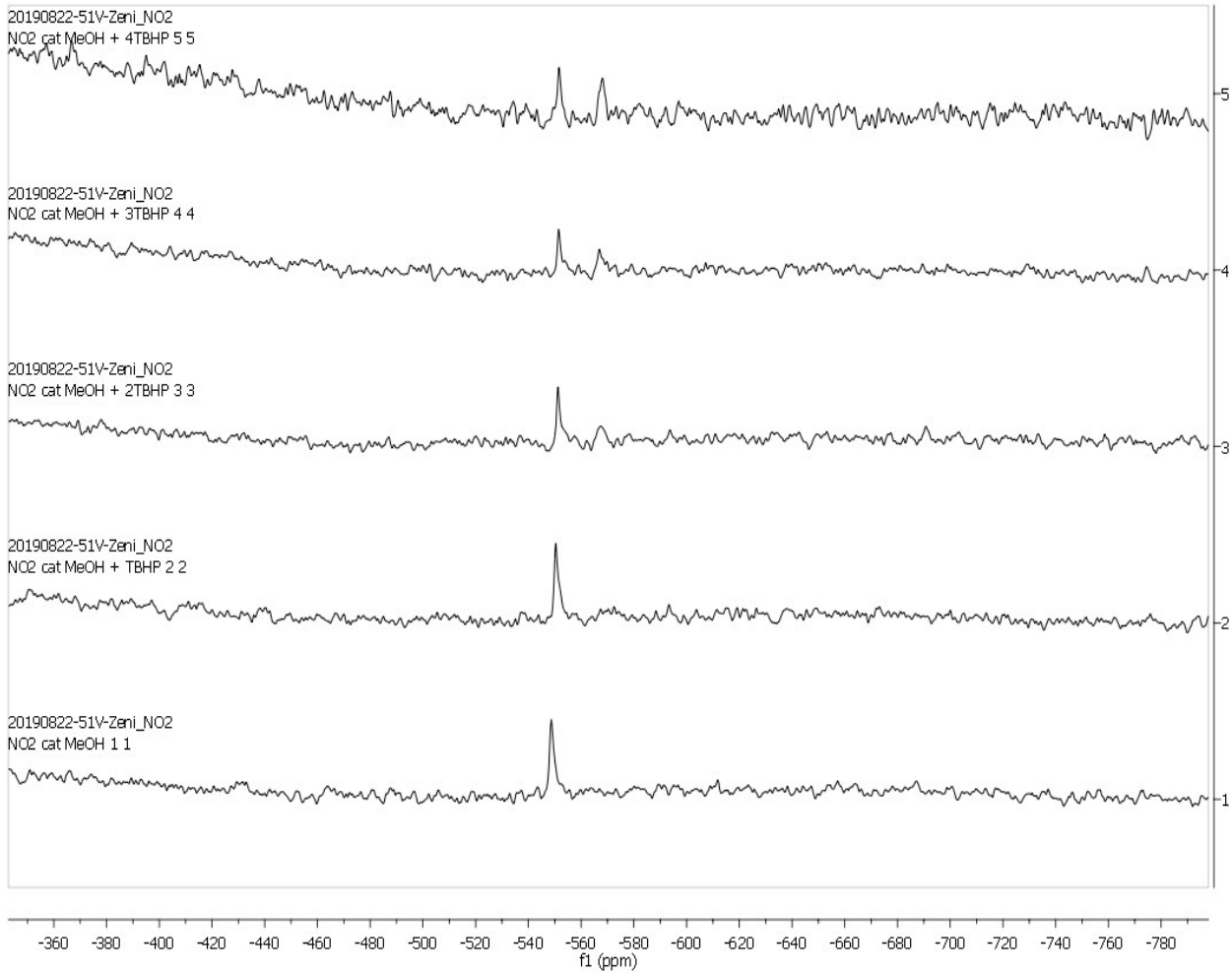

Figure S23. ^{51}V NMR spectra of solutions containing [$V^{IV}O(PIMNO_2)_2$] (concentration < 3 mM) in MeOH:toluene (90:10) after a few hours in air and upon successive additions of *t*-BuOOH. Peaks are initially detected at δ_V = -551 and -568 after additions of *t*-BuOOH; probably these correspond to isomers of [$V^{V}O(PIMNO_2)_2$].

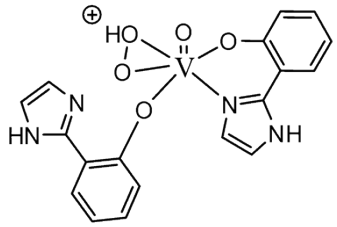 **d1** δ_V^{calc}(MeOH) = -424 ppm δ_V^{calc}(CH_3CN) = -420 ppm δ_V^{calc}(heptane) = -415 ppm G_r: 20.7, 22.5, 22.8, 23.9	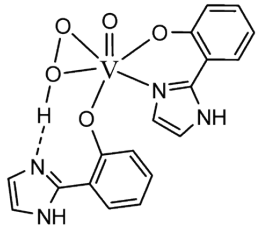 **d2** During calculation it was transformed to **d4**.	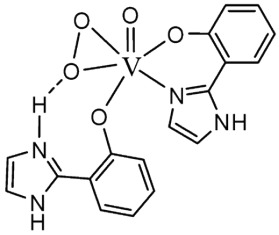 **d4** δ_V^{calc}(MeOH) = -594 ppm δ_V^{calc}(CH_3CN) = -577 ppm δ_V^{calc}(heptane) = -564 ppm G_r: 0.9, 0.4, 0.0, 3.2
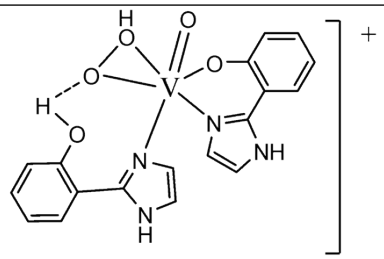 **d3** δ_V^{calc}(MeOH) = -650 ppm δ_V^{calc}(CH_3CN) = -638 ppm δ_V^{calc}(heptane) = -625 ppm	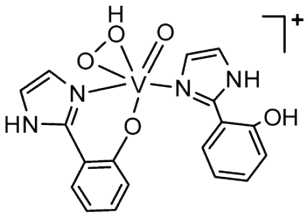 **d3a** δ_V^{calc}(MeOH) = -658 ppm δ_V^{calc}(CH_3CN) = -633 ppm δ_V^{calc}(heptane) = -620 ppm	**d3** is more stable than **d3a** by 5.9 kcal·mol^{-1} in CH_3CN, by 3.7 kcal·mol^{-1} in MeOH and by 4.5 kcal·mol^{-1} in heptane.
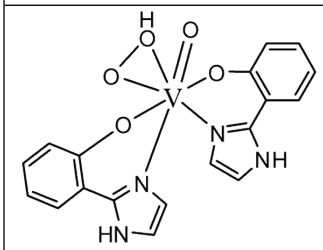 **d5** δ_V^{calc}(MeOH) = -528 ppm δ_V^{calc}(CH_3CN) = -524 ppm δ_V^{calc}(heptane) = -516 ppm G_r: 5.4, 6.8, 9.0, 7.0	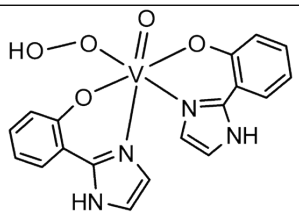 **d5a** δ_V^{calc}(MeOH) = -385 ppm δ_V^{calc}(CH_3CN) = -379 ppm δ_V^{calc}(heptane) = -355 ppm G_r: 0.0, 0.0, 3.4, 0.0	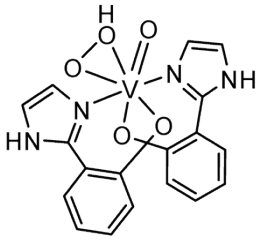 **d5b** δ_V^{calc}(MeOH) = -663 ppm δ_V^{calc}(CH_3CN) = -659 ppm δ_V^{calc}(heptane) = -651 ppm G_r: 3.6, 7.0, 11.2, 6.0

Figure S24. Some of the molecular structures that may be envisaged for $V^VO(HOO)$-complexes; in several cases charges were omitted. The DFT calculated ^{51}V NMR chemical shifts and relative Gibbs free energies (G_r, in kcal·mol^{-1}), when comparable, are indicated. The relative energies given are in sequence: gas phase, CH_3CN solution, MeOH solution and heptane solution. Note that

d5a is more stable than **d5**, but its δ_V^{calc} is too negative to be considered as a plausible species, as no resonances were found below ca. |-550| ppm in solutions where peroxides are present.

Table S5. The calculated chemical shifts for species corresponding to **b3** and **c** are included for complexes $[V^{IV}O(PIMH)_2]$, $[V^{IV}O(PIMNO_2)_2]$, $[V^{IV}O(PIMBr)_2]$ and $[V^{IV}O(PIMMeO)_2]$.

Complex (sutructure and substituent)	δ_V^{calc} in CH_3CN	δ_V^{calc} in MeOH
b-NO_2	-526 ppm	-558 ppm
b3-H	-523 ppm	-567 ppm
b-Br	-526 ppm	-555 ppm
b-OMe	-523 ppm	-547 ppm
c-NO_2	-553 ppm	-583 ppm
c-H	-568 ppm	-594 ppm
c-Br	-561 ppm	-589 ppm
c-OMe	-560 ppm	-583 ppm

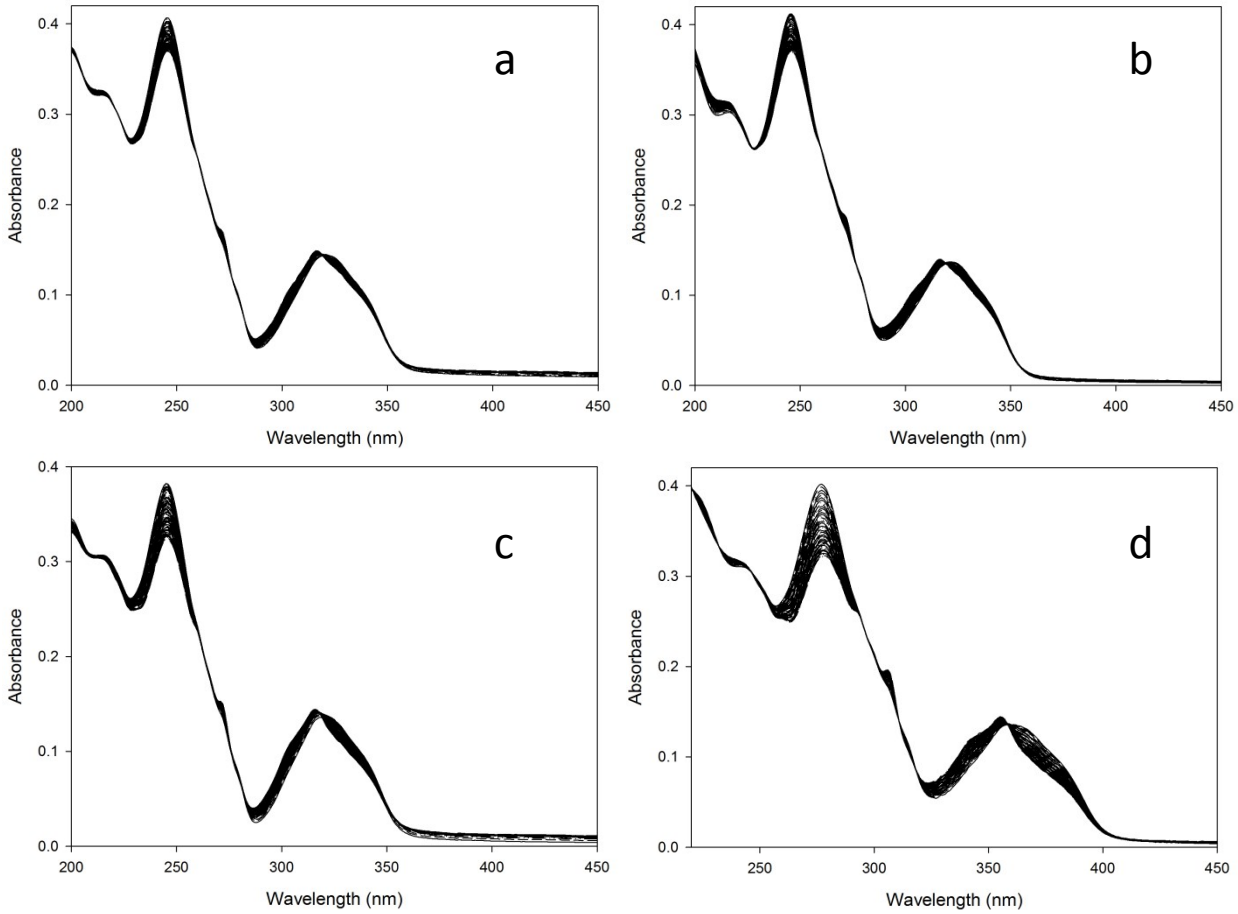

Figure S25. UV-Vis absorbance changes as a function of time at 293.1 K when mixing 0.01004 mM [$V^{IV}O(PIMH)_2$] with (a) 0.005020 mM oxidant, (b) 0.01004 mM oxidant, (c) 0.02008 mM oxidant and (d) 0.03012 mM oxidant.

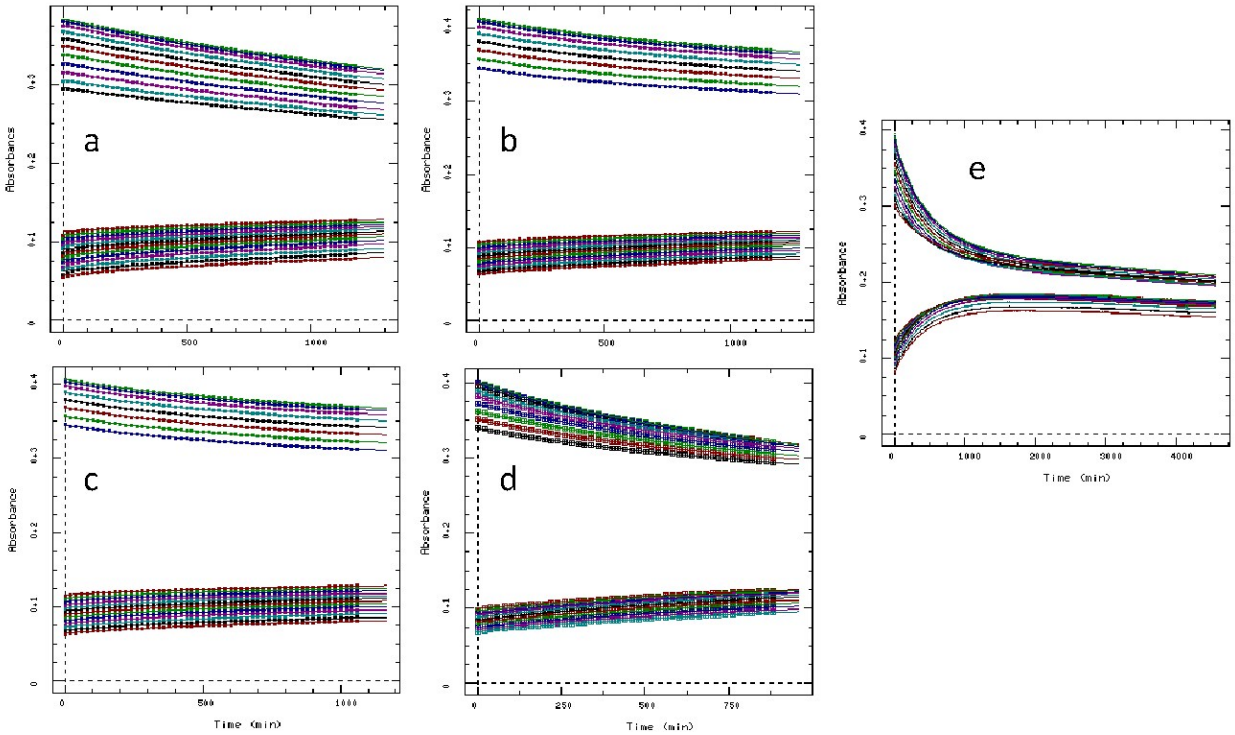

Figure S26. Experimental UV-Vis absorbance changes (symbols) and global non-linear least-squares fits (solid lines) for wavelengths in the range of 236-245 and 298-310 nm as a function of time at 293.1 K when mixing 0.01004 mM [$V^{IV}O(PIMH)_2$] with (a) 0.005020 mM oxidant, (b) 0.01004 mM oxidant, (c) 0.02008 mM oxidant, (d) 0.03012 mM oxidant and (e) 0.06997 mM oxidant.

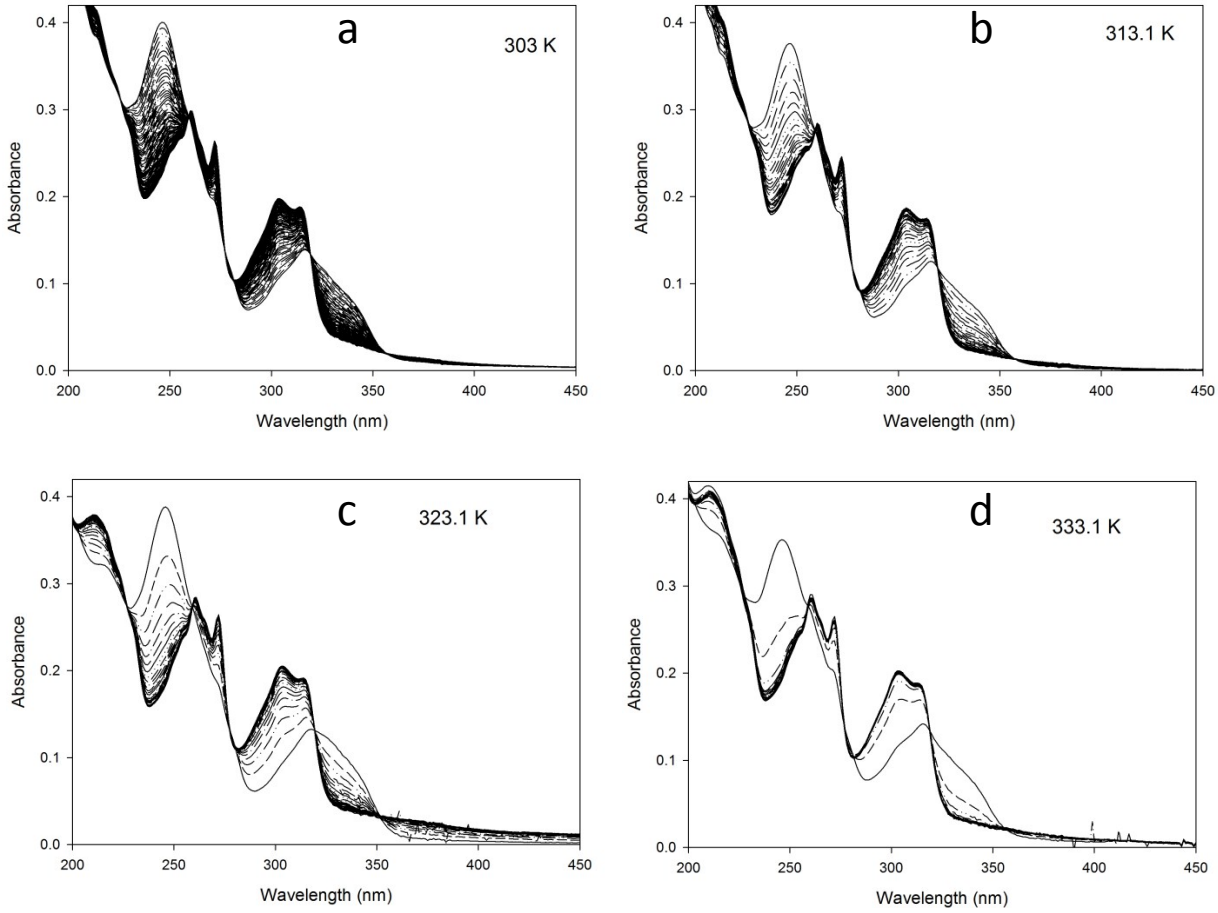

Figure S27. UV-Vis absorbance changes as a function of time and temperature when mixing 0.01004 mM [$V^{IV}O(PIMH)_2$] with 0.03502 mM oxidant.

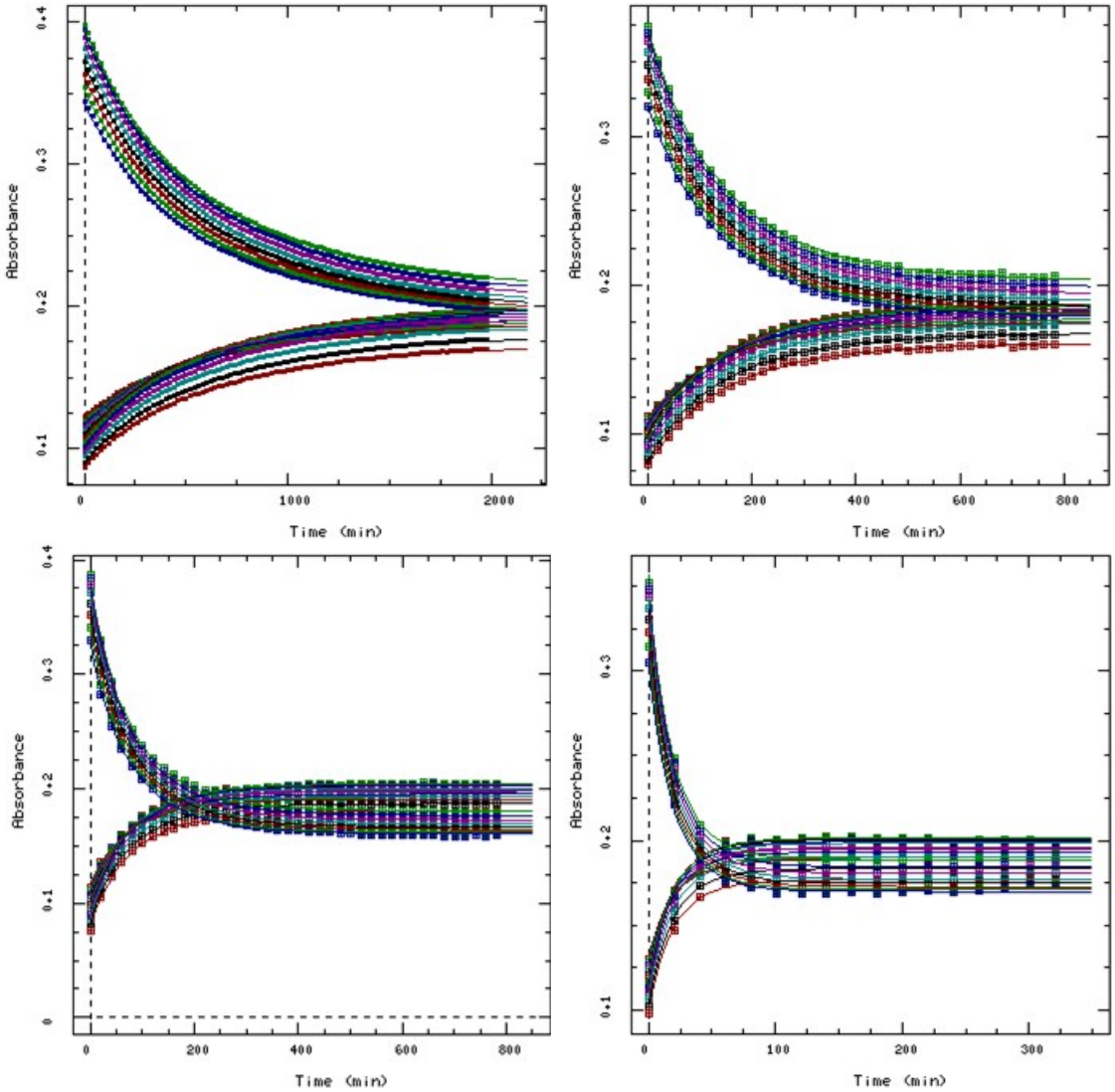

Figure S28. Experimental UV-Vis absorbance changes (symbols) and non-linear least-squares fits (solid lines) for wavelengths in the range of 236-245 and 298-310 nm as a function of temperature when mixing 0.01004 mM [$V^{IV}O(PIMH)_2$] with 0.03502 mM oxidant where (a) 303.1 K, (b) 313.1 K, (c) 323.1 K and (d) 333.1 K.

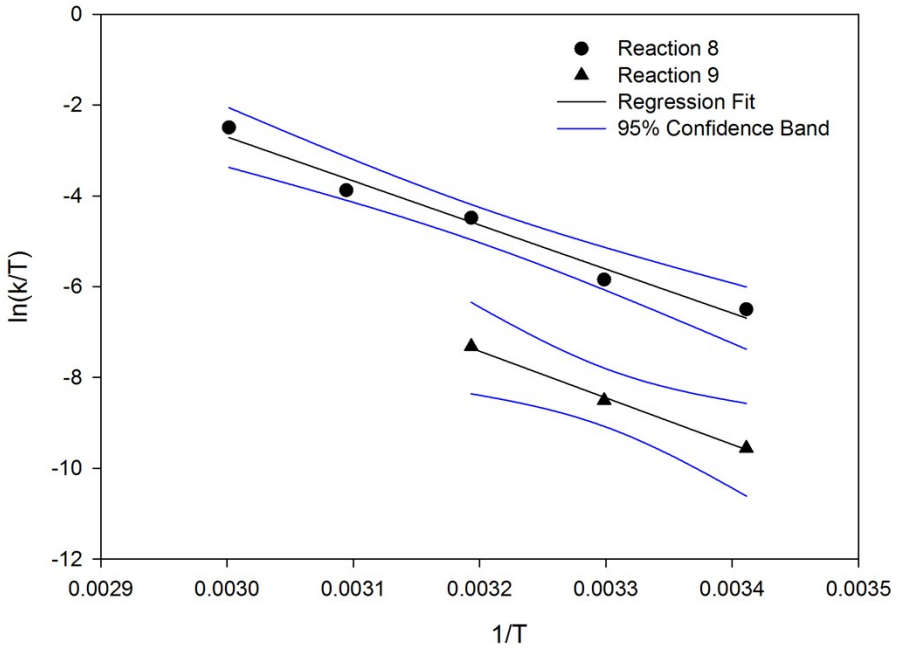

Figure S29. Eyring plots for reactions 8 and 9.

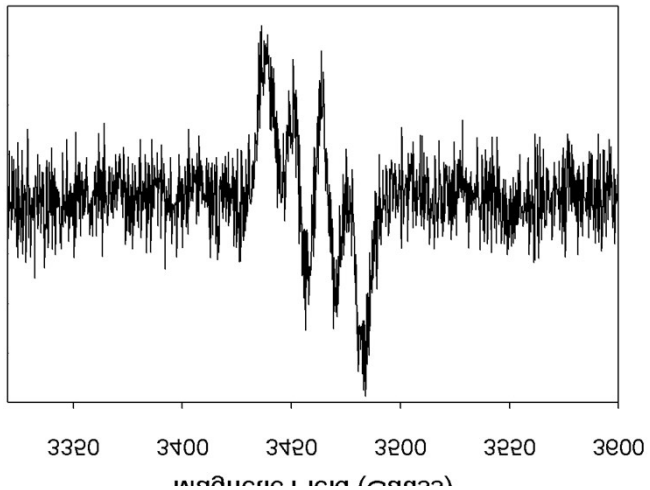

Figure S30. EPR spectrum of the DMPO/• free radical species obtained after immediately adding 0.5 mL of 0.100 M DMPO in DMF to 0.500 mL of 0.100 M [$V^{IV}O(PIMH)_2$] and mole eq. 0.526 M *t*-BuOOH in DMSO.

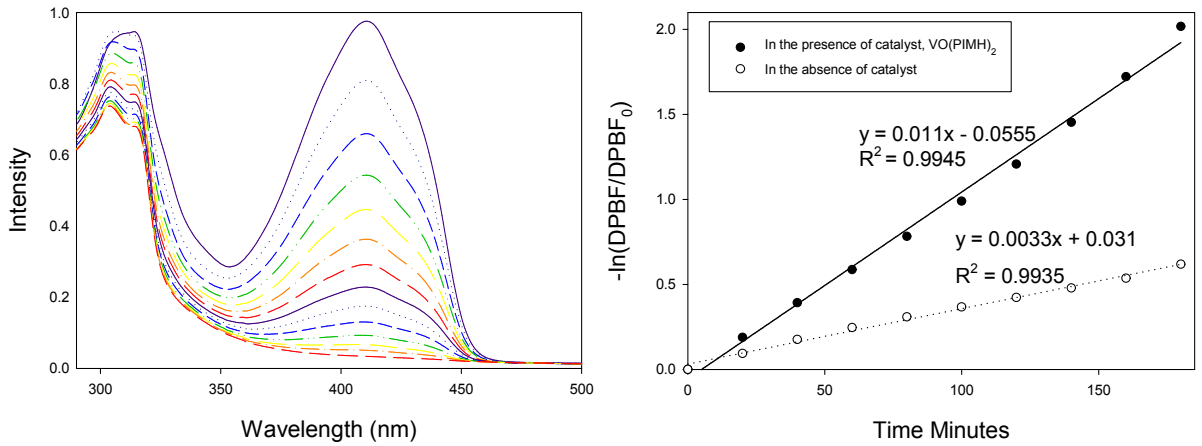

Figure S31. (a) UV-Vis spectra for the decomposition of DPBF in the presence and *t*-BuOOH, and (b) the linear plot comparing the decomposition of DPBF in the presence and in the absence of [$V^{IV}O(PIMH)_2$]. Concentrations; 12.98 nmol catalyst, 14.8 nmol DPBF and 5.26 µmol *t*-BuOOH.

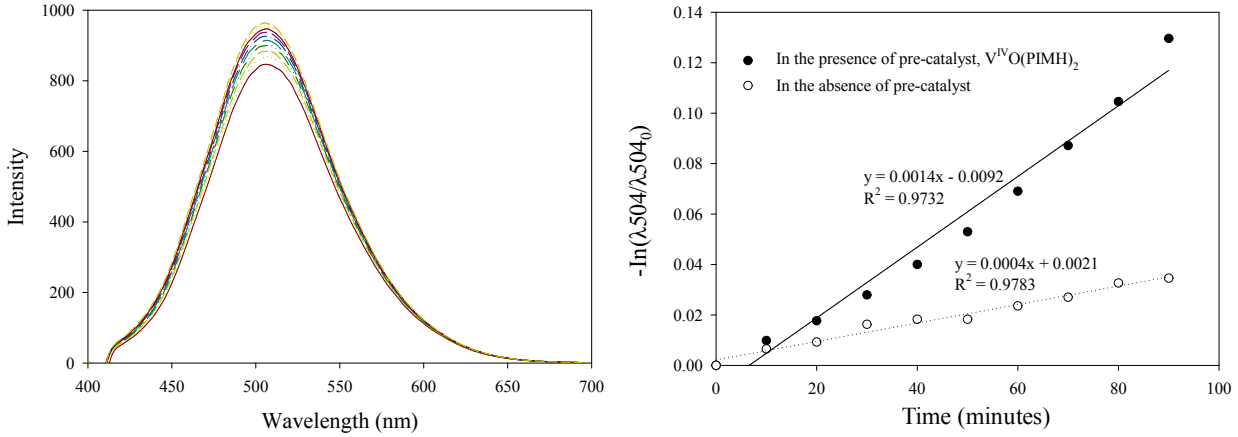

Figure S32. (a) Fluorescence spectra collected every 10 minutes upon mixing 3 mL of furfuryl alcohol with [$V^{IV}O(PIMH)_2$] and t-BuOOH and (b)

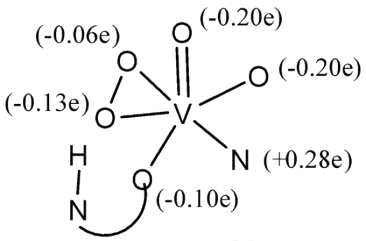

c-H

Sum O-O: -0.19e (in CH_3CN)

-0.12e (in heptane)

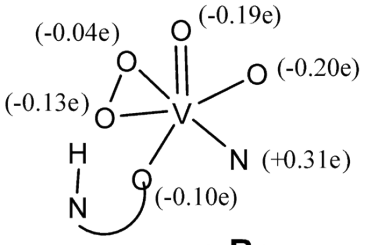

c-Br

Sum O-O: -0.17e (in CH_3CN)

-0.11e (in heptane)

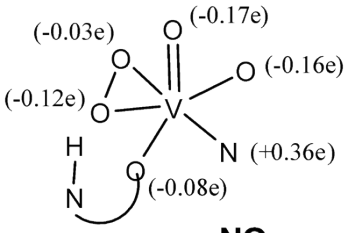

c-NO_2

Sum O-O: -0.15e (in CH_3CN)

-0.08e (in heptane)

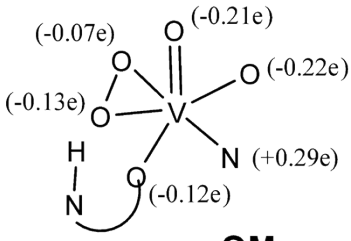

c-OMe

Sum O-O: -0.20e (in CH_3CN)

-0.13e (in heptane)

Figure S33. Mulliken charges calculated for the donor atoms of the peroxido complexes **c-X** (in CH_3CN). The trend in reactivity observed cannot be explained from this data. The sum of the Mulliken charges of the two O-peroxido atoms in CH_3CN and heptane is also indicated.